

Aerosol extinction coefficients at ambient conditions

P. Zieger et al.

[Title Page](#)[Abstract](#)[Introduction](#)[Conclusions](#)[References](#)[Tables](#)[Figures](#)[Back](#)[Close](#)[Full Screen / Esc](#)[Printer-friendly Version](#)[Interactive Discussion](#)

⁵Belgium Institute for Space Aeronomy, Ringlaan 3, 1180 Brussels, Belgium

⁶University of Heidelberg, Institute of Environmental Physics, Im Neuenheimer Feld 229, 69120 Heidelberg, Germany

⁷Japan Agency for Marine-Earth Science and Technology, Research Institute for Global Change, Yokohama, Japan

⁸Max-Planck-Institute for Chemistry, Joh.-Joachim-Becher-Weg 27, 5512 Mainz, Germany

⁹National Institute for Public Health and the Environment RIVM, 3721 Bilthoven, The Netherlands

¹⁰Royal Netherlands Meteorological Institute KNMI, 3730 AE De Bilt, The Netherlands

Received: 1 November 2010 – Accepted: 30 November 2010 – Published: 6 December 2010

Correspondence to: E. Weingartner (ernest.weingartner@psi.ch)

Published by Copernicus Publications on behalf of the European Geosciences Union.

Abstract

In the field, aerosol in-situ measurements are often performed under dry conditions (relative humidity $RH < 30\text{--}40\%$). Since ambient aerosol particles experience hygroscopic growth at enhanced RH, also their microphysical and optical properties – especially the aerosol light scattering – are strongly dependent on RH. The knowledge of this RH effect is of crucial importance for climate forcing calculations or for the comparison of remote sensing with in-situ measurements. Here, we will present results from a four-month campaign which took place in summer 2009 in Cabauw, The Netherlands. The aerosol scattering coefficient $\sigma_{sp}(\lambda)$ was measured dry and at various, predefined RH conditions between 20 and 95% with a humidified nephelometer. The scattering enhancement factor $f(RH, \lambda)$ is the key parameter to describe the effect of RH on $\sigma_{sp}(\lambda)$ and is defined as $\sigma_{sp}(RH, \lambda)$ measured at a certain RH divided by the dry $\sigma_{sp}(dry, \lambda)$. The measurement of $f(RH, \lambda)$ together with the dry absorption measurement (assumed not to change with RH) allows the determination of the actual extinction coefficient $\sigma_{ep}(RH, \lambda)$ at ambient RH. In addition, a wide range of other aerosol properties were measured in parallel. The measurements were used to characterize the effects of RH on the aerosol optical properties. A closure study showed the consistency of the aerosol in-situ measurements. Due to the large variability of air mass origin (and thus aerosol composition) a simple parameterization of $f(RH, \lambda)$ could not be established. If $f(RH, \lambda)$ needs to be predicted, the chemical composition and size distribution needs to be known. Measurements of four MAX-DOAS (multi-axis differential optical absorption spectroscopy) instruments were used to retrieve vertical profiles of $\sigma_{ep}(\lambda)$. The values of the lowest layer were compared to the in-situ values after conversion of the latter to ambient RH. The comparison showed a good correlation of $R^2 = 0.62\text{--}0.78$, but the extinction coefficients were a factor of 1.5–3.4 larger than the in-situ values. Best agreement is achieved for a few cases characterized by low aerosol optical depths and low planetary boundary layer heights. Differences showed to be dependent on the applied MAX-DOAS retrieval algorithm. The comparison of the in-situ data to a Raman

Aerosol extinction coefficients at ambient conditions

P. Zieger et al.

Title Page

Abstract

Introduction

Conclusions

References

Tables

Figures

◀

▶

◀

▶

Back

Close

Full Screen / Esc

Printer-friendly Version

Interactive Discussion



lidar (light detection and ranging) showed a good correlation and higher values measured by the lidar ($R^2 = 0.79$, slope of 1.81) if the Raman retrieved profile was used to extrapolate the directly measured extinction coefficient to the ground. The comparison improved if only nighttime measurements were used in the comparison ($R^2 = 0.93$, slope of 1.19).

1 Introduction

Atmospheric aerosol particles change in size due to water uptake which is determined by their chemical composition and the ambient relative humidity (RH). As a result also their optical properties – especially the aerosol light scattering – strongly depend on RH. Therefore, long-term measurements of aerosol physical and optical properties are generally recommended at dry conditions in order to keep measurements comparable (e.g. RH < 30–40% as recommended by WMO/GAW, 2003). However, for the comparison of such ground-based measurements with other optical aerosol measurements (e.g. lidar, MAX-DOAS or satellite retrieval), for the purpose of aerosol correction of satellite retrievals, or for the use in climate models, accurate knowledge of the RH effect is very important.

The size and the solubility of a particle determine the response of an ambient particle to changes in RH. The water vapor pressure above a water droplet containing dissolved material is lowered by the Raoult effect. The equilibrium size of a droplet was first described by Köhler (1936), who considered the Kelvin (curvature) and Raoult (solute) effect. The growth of an aerosol particle due to water uptake is described by the hygroscopic growth factor $g(\text{RH})$ which is defined as the particle diameter D_{wet} at a certain RH divided by its dry diameter D_{dry} :

$$g(\text{RH}) = \frac{D_{\text{wet}}(\text{RH})}{D_{\text{dry}}}. \quad (1)$$

Aerosol extinction coefficients at ambient conditions

P. Zieger et al.

Title Page

Abstract

Introduction

Conclusions

References

Tables

Figures

◀

▶

◀

▶

Back

Close

Full Screen / Esc

Printer-friendly Version

Interactive Discussion



The RH dependence of $g(\text{RH})$ can be parameterized in a good approximation by a one-parameter equation, proposed e.g. by Petters and Kreidenweis (2007):

$$g(a_w) = \left(1 + \kappa \frac{a_w}{1 - a_w}\right)^{\frac{1}{3}}. \quad (2)$$

Here, a_w is the water activity, which can be replaced by the relative humidity RH, if the Kelvin effect is negligible, as for particles with sizes relevant for light scattering and absorption, i.e. with $D_{\text{wet}} > 100$ nm. The coefficient κ is a simple measure of the particle's hygroscopicity and captures all solute properties (Raoult effect). The impact of hygroscopic growth on the aerosol light scattering coefficient is usually described by the scattering enhancement factor $f(\text{RH}, \lambda)$:

$$f(\text{RH}, \lambda) = \frac{\sigma_{\text{sp}}(\text{RH}, \lambda)}{\sigma_{\text{sp}}(\text{dry}, \lambda)}, \quad (3)$$

where the scattering coefficient σ_{sp} depends on the wavelength λ and the relative humidity RH. In the following we will discuss the characteristics of the scattering enhancement factor for $\lambda = 550$ nm. Since no clear wavelength dependency was found during our measurement period (in the range of 450–700 nm), we will omit λ for simplicity and refer to the scattering enhancement factor as $f(\text{RH})$.

Measured and modeled enhancement factors have been described in several previous studies, including studies on urban (Yan et al., 2009; Fitzgerald et al., 1982), continental (Sheridan et al., 2001), biomass burning (Kotchenruther and Hobbs, 1998), maritime (Fierz-Schmidhauser et al., 2010b; Wang et al., 2007; Carrico et al., 2003), free tropospheric (Fierz-Schmidhauser et al., 2010a; Nessler et al., 2005a) or Arctic aerosol (Zieger et al., 2010).

The comparison of remote sensing measurements to in-situ values of the aerosol extinction for validation purposes has been performed in several studies. Lidar measurements have been compared to nephelometer measurements, but always with dry nephelometer data using model assumptions or literature values of $f(\text{RH})$ (Ferrare et

Aerosol extinction coefficients at ambient conditions

P. Zieger et al.

Title Page

Abstract

Introduction

Conclusions

References

Tables

Figures

◀

▶

◀

▶

Back

Close

Full Screen / Esc

Printer-friendly Version

Interactive Discussion



Aerosol extinction coefficients at ambient conditions

P. Zieger et al.

[Title Page](#)[Abstract](#)[Introduction](#)[Conclusions](#)[References](#)[Tables](#)[Figures](#)[⏪](#)[⏩](#)[◀](#)[▶](#)[Back](#)[Close](#)[Full Screen / Esc](#)[Printer-friendly Version](#)[Interactive Discussion](#)

al., 1998; Voss et al., 2001) and only rarely using a humidified nephelometer (Morgan et al., 2010). The MAX-DOAS technique for aerosol retrieval is novel and only few comparisons have been made with in-situ data. The first comparison of the extinction coefficient (measured at Ghuangzhou, China) with a single MAX-DOAS instrument (similar retrieval as for the MPI instrument, see below) to nephelometer data was made by Li et al. (2010) using a single parameterization from a different station (60 km further away) to calculate the ambient extinction coefficients from the dry nephelometer data. In addition, they only used ground based RH measurements and differences between indoor and ambient RH and temperature conditions were not accounted for.

In this study, the RH dependency of the aerosol extinction coefficient was examined using direct measurements of aerosol optical properties as a function of RH taken during a four months campaign at Cabauw, The Netherlands. The data was compared in an optical closure study with Mie-calculations, which relied on the aerosol number size distribution corrected to a specific RH using hygroscopicity measurements. As a proof of concept, the in-situ measurements were compared to remote sensing data from MAX-DOAS and lidar measurements. The vertical profiles of the aerosol extinction obtained from MAX-DOAS and their comparison to LIDAR measurements are discussed in an accompanying publication (Frieß et al., 2010).

2 The Cabauw site and the CINDI campaign

A field campaign was carried out from 8 June to 6 October 2009 at the Cabauw Experimental Site for Atmospheric Research (CESAR, located at 51.97° N, 4.93° E) in The Netherlands. The site is located approx. 33 km east of the city of Rotterdam and 30 km west of Utrecht. CESAR is a facility dedicated to the observation and characterization of the state of the atmosphere, its radiative properties and interaction with land surface, for the study of physical processes, climate monitoring and validation studies (Ruschchenberg et al., 2005). A large set of continuous in-situ and remote sensing equipment is installed at the site. A 213 m high mast equipped with various meteorological

sensors (like temperature, dew point, wind direction, wind speed, etc.) is the main feature of the CESAR site. The continuous aerosol measurements are contributing to the EUSAAR (European Supersites for Atmospheric Aerosol Research) project (Philippin et al., 2009) with associated quality control, site audits, and reporting.

5 During 16 June and 24 July 2009 our measurements were part of the CINDI campaign (Cabauw Intercomparison Campaign of Nitrogen Dioxide measuring Instruments) where the main goal was to compare different remote sensing and in-situ techniques measuring NO_2 . Besides NO_2 , other atmospheric gases and aerosols were measured and intercompared. For more details see Roscoe et al. (2010) and Piters et al. (2010).

3 Experimental

Various physical and chemical aerosol properties have been measured during the four-month period. The following section describes the main experimental techniques used in this work. In the first part (Sect. 3.1) the main in-situ instruments used to characterize the effects of RH on the aerosol extinction coefficient will be described. The results of the in-situ measurements are later compared to two different atmospheric profiling techniques: First to MAX-DOAS measurements (Sect. 3.2) and in a next step to lidar measurements (Sect. 3.3). This comparison is carried out only for the lowest layer.

3.1 In-situ measurements

3.1.1 Inlet system

Air is sampled at a height of 60 m at the Cabauw tower. The inlet system consists of four parts: (a) PM_{10} size selective inlets (4 PM_{10} heads), (b) a Nafion drying system that dries aerosol to or below 40% RH, (c) a 60-m stainless steel pipe, and (d) a manifold that splits the flow to the suite of instruments. The manifold and the in-situ

Aerosol extinction coefficients at ambient conditions

P. Zieger et al.

Title Page

Abstract

Introduction

Conclusions

References

Tables

Figures

◀

▶

◀

▶

Back

Close

Full Screen / Esc

Printer-friendly Version

Interactive Discussion



instruments are all located at the basement of the tower. The in-situ measurements used in this paper are those from the nephelometer, MAAP, aethalometer, SMPS and APS, all of which are described below. These instruments sampled their flow from the manifold using separate pumps to adjust the required flow for proper operation of the instruments.

The total flow sustained in the 60-m inlet pipe was 60 lpm, for optimal operation of the PM₁₀ inlets. Whenever an instrument was added or removed, the flows to the other instruments were checked and adjusted when needed. Although attempts have been made to characterize the losses, they were not conclusive. In general the losses in similar inlet pipes are according to theory (e.g., Birmili et al., 2007). Additional losses are expected due to the use of a Nafion dryer but there is no quantitative information for the specific dryer used in Cabauw.

3.1.2 Humidified and dry nephelometer

A recently developed humidified nephelometer (WetNeph) was installed for four months next to the continuously running aerosol in-situ instruments. The WetNeph is described in detail by Fierz-Schmidhauser et al. (2010c). Briefly, the aerosol scattering coefficient $\sigma_{sp}(\lambda)$ and the back scattering coefficient $\sigma_{bsp}(\lambda)$ are measured at three wavelengths ($\lambda = 450, 550, \text{ and } 700 \text{ nm}$) at defined RH between 20% and 95%. For this purpose a specifically designed single-stream humidification system (consisting of a humidifier and followed by a dryer) brings the initially dry aerosol (the aerosol is already dried at the main inlet) to a defined RH before its scattering properties are measured by an integrating nephelometer (TSI Inc., Model 3563).

The WetNeph was programmed to measure RH cycles. In the first part of the cycle, the dry particles experience elevated RH in the humidifier, after which they are passed through the turned off dryer before their scattering properties are measured in the nephelometer (hydration mode). It is noted that the temperature in the nephelometer's detection cell is $\sim 1^\circ\text{C}$ higher than in the humidifier, thereby causing a slight RH decrease of approximately 2–6% (see Fig. A1 in Fierz-Schmidhauser et al., 2010c)

Aerosol extinction coefficients at ambient conditions

P. Zieger et al.

Title Page

Abstract

Introduction

Conclusions

References

Tables

Figures

◀

▶

◀

▶

Back

Close

Full Screen / Esc

Printer-friendly Version

Interactive Discussion



Aerosol extinction coefficients at ambient conditions

P. Zieger et al.

Title Page

Abstract

Introduction

Conclusions

References

Tables

Figures

◀

▶

◀

▶

Back

Close

Full Screen / Esc

Printer-friendly Version

Interactive Discussion



and with that a concurrent shift of the observed deliquescence RH. Deliquescence is known as a sudden uptake of water of an initially dry and solid particle at the defined deliquescence relative humidity (DRH). Inorganic salts (for instance ammonium sulfate or sodium chloride) exhibit a distinct deliquescence. Organic constituents of mixed atmospheric aerosols can suppress the deliquescence of the inorganic salts (Sjogren et al., 2007). The behavior of dehydrating particles following the upper hysteresis branch of the growth curve is measured by setting the humidifier to its maximum RH (~95%), followed by RH reduction in the dryer and measurement in the nephelometer (dehydration mode). The lowest possible RH in this mode was ~55%, limited by the capacity of the dryer at the high sample flow of 10 l min⁻¹ chosen for this campaign.

A second nephelometer (DryNeph, TSI Inc., Model 3563, operated by TNO) was used in parallel to measure the scattering coefficient under dry conditions as a reference. The RH inside the DryNeph was always below 30% (campaign mean RH = 17.7%).

Both nephelometers measured within the scattering angles of 7° to 170°. The scattering coefficients for the complete angle between 0° and 180° were retrieved by correcting the measured values using the scheme proposed by Anderson et al. (1996) (truncation error correction).

3.1.3 Measurement of the aerosol absorption coefficient

A multi-angle absorption photometer (MAAP) and an aethalometer were used to quantify the aerosol absorption properties.

The MAAP (Thermo Scientific Inc., Model 5012, operated by TNO) measures the light attenuation and light scattered back from aerosol particles which are deposited on a filter. The measurement is performed at $\lambda = 637$ nm (which differs from the manufacturer's value of 670 nm, Müller et al., 2010). A radiative transfer scheme is applied to retrieve the fraction of light absorbed by the deposited aerosol (Petzold and Schönlinner, 2004). The aerosol absorption coefficient σ_{ap} is obtained by multiplying the measured black carbon (BC) mass concentration with the instrumental set value of the mass absorption cross section of $6.6 \text{ m}^2 \text{ g}^{-1}$.

In addition, an aethalometer (Magee Scientific, Model AE-31, operated by RIVM) was used which measures the light attenuation by the aerosol particles (also deposited on a filter) at 7 wavelengths ($\lambda = 370, 470, 520, 590, 660, 880, \text{ and } 950 \text{ nm}$). The aerosol absorption coefficient $\sigma_{\text{ap}}(\lambda)$ is then derived from the light attenuation:

$$\sigma_{\text{ap}}(\lambda) = \frac{A}{Q} \frac{\Delta \text{ATN}(\lambda)}{\Delta t} \frac{1}{C \cdot R(\text{ATN}(\lambda))}, \quad (4)$$

where A is the filter spot area, Q the volumetric flow, and $\Delta \text{ATN}(\lambda)$ the change of light attenuation during the time interval Δt (Weingartner et al., 2003). The empirical constant C corrects for multiple scattering in the unloaded filter. Here, a value of $C = 4.09$ was used (Collaud Coen et al., 2010). The wavelength and ATN dependent factor R corrects for effects caused by the amount of particles deposited on the filter, which decrease the optical path in the filter (also called the shadowing effect). R was set to unity as the single scattering albedo ω_0 (defined as the ratio of scattering to extinction coefficient) is larger than 0.8 for most of the times (Weingartner et al., 2003).

Since the aethalometer measures at various wavelengths, the absorption Ångström exponent α_{ap} can be derived:

$$\sigma_{\text{ap}}(\lambda) = \epsilon \lambda^{-\alpha_{\text{ap}}}, \quad (5)$$

where λ is the wavelength of the aethalometer and ϵ a concentration dependent constant.

Using the measured α_{ap} of the aethalometer and the measured value of $\sigma_{\text{ap}}(637 \text{ nm})$ from the MAAP, the absorption coefficient for a different wavelength λ was calculated as follows:

$$\sigma_{\text{ap}}(\lambda) = \sigma_{\text{ap}}(637 \text{ nm}) \left(\frac{\lambda}{637 \text{ nm}} \right)^{-\alpha_{\text{ap}}}. \quad (6)$$

Aerosol extinction coefficients at ambient conditions

P. Zieger et al.

Title Page	
Abstract	Introduction
Conclusions	References
Tables	Figures
◀	▶
◀	▶
Back	Close
Full Screen / Esc	
Printer-friendly Version	
Interactive Discussion	



3.1.4 Measurement of the aerosol size distribution

A scanning mobility particle sizer (SMPS) and an aerodynamic particle sizer (APS) were used to measure the aerosol size distribution for dry diameters between approx. 10 nm and 5 μm (both operated by TNO).

5 The SMPS (a modified TSI Inc., Model 3034) consists of a bipolar particle charger, a differential mobility analyzer (DMA) and a condensation particle counter (CPC). Particles are charged before they are classified in the DMA according to their electrical mobility diameter and are counted in the CPC. A correction for multiple charged particles was applied. Number size distributions in the diameter range between approx. 10
10 and 520 nm were recorded with a time resolution of 5 min.

The APS (TSI Inc., Model 3321) measures the particle size distribution between aerodynamic diameters of approx. 0.5 and 20 μm . However, in Cabauw, particles larger than approx. 5 μm are not sampled through the inlet system due to the PM_{10} size cut at the inlet and the drying thereafter, which goes along with a reduction in size. One
15 distribution is recorded each minute.

3.1.5 Measurement of the hygroscopic growth factor

Hygroscopic particles are able to grow in size by absorbing water vapor even in sub-saturated conditions. A simple way to describe the hygroscopicity of a particle is via the diameter growth factor g as defined in Eq. (1). This property can be measured
20 directly with a hygroscopicity tandem differential mobility analyzer (H-TDMA, Liu et al., 1978). The aerosol sample is first dried in the H-TDMA, and then charged with a bipolar charger. Subsequently a dry size class of particles, D_{dry} , is selected using a DMA (Winklmayr et al., 1991). At Cabauw, the H-TDMA of the University of Helsinki (modified version of the instrument presented by Ehn et al., 2007) was set to measure
25 D_{dry} of 35, 50, 75, 110, and 165 nm. Then the monodisperse particles are brought into controlled relative humidity (90%) and temperature. The wet aerosol goes through the second DMA, which scans a size range covering possible growths factors from 0.7 to

Aerosol extinction coefficients at ambient conditions

P. Zieger et al.

Title Page

Abstract

Introduction

Conclusions

References

Tables

Figures

◀

▶

◀

▶

Back

Close

Full Screen / Esc

Printer-friendly Version

Interactive Discussion



2.5. A corresponding concentration for each size fraction is monitored with a CPC. A humidified size distribution for a certain D_{dry} is then obtained.

When measuring the hygroscopicity of an aerosol population, a distribution of different growth factors is usually obtained instead of a single value (Swietlicki et al., 2008).

This is due the fact that hygroscopic properties are mainly governed by the chemical composition and the size of the particles. In the case of highly variable and externally mixed ambient aerosol populations in Cabauw the Piecewise Linear method of the TDMAinv Toolkit (Gysel et al., 2008) was used to retrieve the growth factor distributions. For this work, only the largest dry size (165 nm) was used, and during the entire analyzed period, the growth distribution was dominated by one mode. Therefore, simply using the average growth factor is sufficient.

3.2 MAX-DOAS measurements

Multi-axis differential optical absorption spectroscopy (MAX-DOAS) is a technique to derive profiles of atmospheric gases and aerosols using spectral radiation measurements under different (mostly slant) elevation angles (Hönninger and Platt, 2002; Leser et al., 2003; Van Roozendaal et al., 2003; Wittrock et al., 2004; Hönninger et al., 2004; Wagner et al., 2004; Sinreich et al., 2005; Heckel et al., 2005; Frieß et al., 2006; Irie et al., 2008).

For the retrieval of aerosol extinction profiles, usually the atmospheric absorption of the oxygen collision-induced dimer ($\text{O}_2\text{-O}_2$ or O_4) is analyzed. Since the atmospheric O_2 concentration is almost constant, changes in the observed absorption can be attributed to changes in the atmospheric radiative transfer, e.g. caused by the influence of aerosol scattering and absorption (Wagner et al., 2004; Frieß et al., 2006). By comparison with a forward model which describes the effects of aerosols on the MAX-DOAS measurements, aerosol properties can be inverted from the measured O_4 absorption. Usually MAX-DOAS aerosol retrieval consists of two steps: first, the O_4 optical depth is retrieved from the measured spectra using the DOAS technique (Platt and Stutz, 2008). In a second step, the aerosol properties are inverted by comparing

Aerosol extinction coefficients at ambient conditions

P. Zieger et al.

Title Page

Abstract

Introduction

Conclusions

References

Tables

Figures

◀

▶

◀

▶

Back

Close

Full Screen / Esc

Printer-friendly Version

Interactive Discussion



the measured O_4 optical depths to those simulated by a radiative transfer model. As was shown by Frieß et al. (2006) and Clémer et al. (2010), dependent on the wavelength and atmospheric visibility, typically 1–3 independent pieces of information on the aerosol extinction profile can be obtained from MAX-DOAS O_4 observations. It is noted that usually for some of the aerosol optical properties (e.g. the single scattering albedo or the asymmetry parameter) either fixed values are assumed or information from independent measurements (e.g. sun photometers or in-situ measurements) is used.

In this study MAX-DOAS aerosol retrievals from four groups are included: the Belgium Institute for Space Aeronomy (BIRA), the Institute for Environmental Physics of the University of Heidelberg (IUPHD), the Japan Agency for Marine-Earth Science and Technology, Research Institute for Global Change (JAMSTEC), and the Max-Planck-Institute for Chemistry (MPI). All groups use similar retrieval schemes for the spectral analysis of the O_4 absorption (first step); further details of the spectral analysis can be found in Roscoe et al. (2010). For the inversion of the aerosol properties by comparison with radiative transfer simulations (second step) two different approaches are used. BIRA, IUPHD, and JAMSTEC apply the optimal estimation method (Rodgers, 2000), which yields height-resolved profiles of the aerosol extinction coefficient. MPI uses a more simplified approach following the technique of Li et al. (2010): the aerosol extinction profile is described by only two parameters (the total aerosol optical depth and the aerosol layer height) which are determined by fitting the measured O_4 optical depths to the radiative transfer simulations using a least squares method (the aerosol extinction is assumed to be constant within the aerosol layer).

The properties of the different MAX-DOAS measurements and the specific settings of the aerosol inversion schemes are summarized in Table 1. Note that most groups analyze the O_4 absorption band at 477 nm which is close to the wavelengths of the in-situ aerosol measurements. Because of the limited spectral range of the instrument, MPI uses the O_4 band at 360 nm. It should also be noted that some uncertainty with respect to the absolute value of the O_4 absorption cross section exists (Wagner et al.,

Aerosol extinction coefficients at ambient conditions

P. Zieger et al.

Title Page

Abstract

Introduction

Conclusions

References

Tables

Figures

◀

▶

◀

▶

Back

Close

Full Screen / Esc

Printer-friendly Version

Interactive Discussion



2009; Clémer et al., 2010), and all groups apply a correction factor to the retrieved O_4 absorption ranging between 0.75 and 0.83, see Table 1. Additional information on the individual retrievals can be found in a comparison exercise of the spectral analyses during the CINDI campaign (Roscoe et al., 2010) and in a MAX-DOAS aerosol comparison paper by Frieß et al. (2010).

3.3 Lidar measurements

The lidar CAELI (CESAR Water Vapour, Aerosol and Cloud Lidar; Apituley et al., 2009) is a high-performance, multi-wavelength Raman lidar, capable of providing round-the-clock measurements. The instrument is part of the European Aerosol Research Lidar Network (EARLINET), and provides profiles of volume backscatter and extinction coefficients of aerosol particles, the depolarization ratio, and water-vapor-to-dry-air mixing ratio. A high-power Nd:YAG laser transmits pulses at 355, 532, and 1064 nm. Because a large telescope is essentially blind for lidar signals from close to the instrument, a second, small telescope is needed to cover the near range, in particular for measurements in the planetary boundary layer. The lidar echoes at the elastic and Raman scattered wavelengths are relayed to the photo detectors through optical fibers. The lidar returned signals strongly depend on the range h and decrease with h^2 . Multiplication with h^2 thus removes the range dependence. In this way, the range-corrected signals for the vertically pointing ground-based lidar are obtained. Range-corrected signals at 1064 nm are dominated by particle backscatter and are therefore well-suited to display aerosol layering structure and dynamics and to detect the presence of clouds (see e.g. Fig. 7a).

Raman lidars can retrieve aerosol extinction profiles using a single lidar signal at a nitrogen Raman scattered wavelength, with just the help of an atmospheric density profile (e.g. a radio sonde or an atmospheric model) (Ansmann et al., 1992). However, two major problems occur when extinction needs to be calculated at daytime and close to the ground:

Aerosol extinction coefficients at ambient conditions

P. Zieger et al.

Title Page

Abstract

Introduction

Conclusions

References

Tables

Figures

◀

▶

◀

▶

Back

Close

Full Screen / Esc

Printer-friendly Version

Interactive Discussion



Aerosol extinction coefficients at ambient conditions

P. Zieger et al.

Title Page

Abstract

Introduction

Conclusions

References

Tables

Figures

◀

▶

◀

▶

Back

Close

Full Screen / Esc

Printer-friendly Version

Interactive Discussion



1. Raman signals are relatively weak and often dominated by the daylight background, and
2. the geometry of the lidar instrument, the so-called overlap-function, dictates a minimum distance beyond which unbiased extinction values can be derived.

For CAELI, the Raman signals at 387 nm are strong enough for daytime performance up to a few km altitude, however, trustworthy extinction profiles start between 500 and 1000 m above ground.

To work around the overlap problem for this study, extinction profiles were calculated via the Raman aerosol backscatter profiles down to about 60 m above ground. This was achieved by calculating the Raman aerosol backscatter profile from the ratio of the N₂ Raman signal and the elastic (normal) lidar signal (Ansmann et al., 1992). Because both of these signals are affected in the same way by the overlap function, for a well-aligned lidar system, it does not affect their ratio. For CAELI, correct alignment could be verified using methods described by Freudenthaler (2008).

For a given measurement, the Raman backscatter (β) and extinction (σ_{ep}) profiles are calculated. From these profiles the lidar-ratio LR is determined:

$$\text{LR}(h) = \frac{\sigma_{\text{ep}}(h)}{\beta(h)} \quad (7)$$

where h denotes the height above the ground.

The lidar ratio is only valid beyond the minimum overlap height where both σ_{ep} and β are valid. However, it can be argued that within well-mixed states of the boundary layer, LR should be fairly constant, since it is representative for a particular type of aerosol and only RH can be a significant factor determining the LR (Salemink et al., 1984; Ackermann, 1998). So by assuming an effective LR, LR', the backscatter profile at lower altitudes can be converted to an extinction profile using LR' as a conversion factor in Eq. (7). By varying LR' between a range of values and comparing to in-situ measurements, it can be verified whether the values obtained in this way are consistent.

4 Results

The results of the in-situ measurements are presented in the first sections. First, the results of the WetNeph analysis and the factors influencing $f(\text{RH})$ at Cabauw are discussed in Sects. 4.1 and 4.2. A closure study using different aerosol in-situ measurements is shown in Sect. 4.3. How to predict $f(\text{RH})$ without explicit WetNeph measurements at Cabauw is also discussed here. The ambient aerosol extinction coefficient is compared to MAX-DOAS and lidar measurements in Sect. 4.4.

4.1 WetNeph analysis

During the four-month campaign the WetNeph and DryNeph were running continuously without any major interruptions (except for a 70 h break at the end of August). The WetNeph was set to measure humidograms for most of the time, except for two 7 and 11 day long periods in July and August, where the relative humidity was set on a constant value of approx. 82–85%. This was done to further investigate diurnal cycles. Due to the large variation of air masses, no explicit diurnal cycles were found. The humidograms were parameterized with an empirical equation, which has been used in previous studies (Clarke et al., 2002; Carrico et al., 2003) and has been found to best describe the individual branches (hydration, dehydration separately):

$$f(\text{RH}) = a(1 - \text{RH})^{-\gamma}. \quad (8)$$

The humidograms were averaged (3-h mean values for 2% wide RH-bins) and fitted with Eq. (8) for $\text{RH} > 70\%$. No differences were found at this high RH values between the hydration and dehydration branch). During the periods when the WetNeph was operated in a constant RH mode Eq. (8) was used with a campaign mean value for $a = 0.7$ (upper branch only).

Figure 1a shows the temporal evolution of $f(\text{RH})$ for $\text{RH}=85\%$ for the entire campaign period. The values varied between mid June and the beginning of October between approx. 1.3 and 3.9 (10th perc. = 1.32, 90th perc. = 1.52). The corresponding

Aerosol extinction coefficients at ambient conditions

P. Zieger et al.

Title Page

Abstract

Introduction

Conclusions

References

Tables

Figures

◀

▶

◀

▶

Back

Close

Full Screen / Esc

Printer-friendly Version

Interactive Discussion



measured dry and wet (at RH = 85%) scattering coefficients (at 550 nm) and absorption coefficients (at 670 nm) are shown in Fig. 1b. The main contribution to the ambient extinction coefficient (= scattering plus absorption coefficient) is the scattering coefficient, since the absorption coefficient is about an order of magnitude lower than the scattering coefficient.

4.2 Factors influencing $f(\text{RH})$ at Cabauw

$f(\text{RH})$ experienced distinct periods of lowered or elevated values (see Fig. 1a), which were determined by the origin of the air masses as revealed from 48-h air-mass back trajectories which were calculated using the FLEXTRA trajectory model (Stohl et al., 1995; Stohl and Seibert, 1998) and ECMWF (European Centre for Medium Range Weather Forecasts) meteorological data (trajectories are provided by NILU at www.nilu.no/trajectories). The result is shown in Fig. 2a where the back trajectories are color coded by the $f(\text{RH} = 85\%)$ measured at Cabauw. In general, the $f(\text{RH} = 85\%)$ is lower in air masses originating from the continent and urban regions (like Rotterdam or Ruhr area), probably reflecting the presence of aerosol particles with lower hygroscopicity resulting from anthropogenic emissions and lower sea salt content. Air masses which were transported over the North Atlantic Ocean or the North Sea prior to their arrival in Cabauw likely contain more sea-salt leading to higher hygroscopic growth and therefore to higher values of $f(\text{RH} = 85\%)$. Mixtures of both extremes are frequently observed, for example air parcels that have their origin over the Atlantic Ocean and are passing over heavy industrialized areas (like the Rotterdam area or southern Great Britain) where the addition of anthropogenic pollution leads to lower hygroscopicity.

Examples of typical humidograms measured at Cabauw are shown in Fig. 2b–f. These averaged humidograms are sorted according the origin of the air masses arriving at the site. A typical maritime case is presented in Fig. 2b. This humidogram shows a sudden increase of $f(\text{RH})$ at $\sim 65\% \text{RH}$ (deliquescence) during the hydration mode (increase of RH, dark blue circles). During the dehydration mode (humidifier constantly at high RH and dryer on, light blue circles), the deliquescence RH is passed

Aerosol extinction coefficients at ambient conditions

P. Zieger et al.

Title Page

Abstract

Introduction

Conclusions

References

Tables

Figures

◀

▶

◀

▶

Back

Close

Full Screen / Esc

Printer-friendly Version

Interactive Discussion



and $f(\text{RH})$ decreases until $\text{RH} \approx 58\%$. This is not the crystallization RH, which unfortunately can not be measured with our set-up, due to temperature and flow conditions inside the WetNeph (see Sect. 3.1.2). The distinct hysteresis behavior indicates that an almost pure maritime aerosol consisting mainly of inorganic salts – e.g. NaCl – was detected here. Figures 2d and 2e are two further examples of air masses having a maritime origin, although they show no clear deliquescence behavior. While the maritime slightly polluted case (Fig. 2d) reveals a similarly high magnitude of $f(\text{RH})$ as the clear maritime case (Fig. 2b), but without deliquescence, the maritime heavily polluted case is characterized by much lower values of $f(\text{RH})$. This is probably caused by additional pollution and/or a higher fraction of organics, which suppresses the deliquescence and/or reduces the hygroscopic growth of the particles (Ming and Russel, 2001). Figures 2c and 2f show two examples of air masses having a continental origin. Both humidograms show a smooth increase of $f(\text{RH})$ without a distinct deliquescence behavior. This means that the particles are liquid over a broad RH range. The continental south air masses (Fig. 2c) show the lowest values of $f(\text{RH})$ of ~ 1.9 at $\text{RH} = 85\%$. These air parcels originated from northern France, Belgium and The Netherlands south of Cabauw. It is emphasized that these are examples of selected air masses only. A simple categorization can not be established due to the high variability of origin and composition.

What determines the magnitude of $f(\text{RH})$ and what other parameters can be used as proxies to estimate $f(\text{RH})$? To answer these questions, the main in-situ aerosol parameters available during our measurement period were cross-correlated. The result is presented in Fig. 3, which shows the coefficient of determination R^2 (squared correlation coefficient) of $f(\text{RH} = 85\%)$ versus each parameter (the positive or negative sign shows the algebraic sign of the correlation coefficient). The strongest correlation ($R^2 = 0.72$) of $f(\text{RH} = 85\%)$ exists with the hygroscopic growth factor $g(165 \text{ nm})$ measured by the H-TDMA for the dry diameter of 165 nm. The chemical composition of the particle at this rather large diameter is the main factor that determines its ability to grow. This value seems to be the best proxy measured independently that can be

Aerosol extinction coefficients at ambient conditions

P. Zieger et al.

Title Page

Abstract

Introduction

Conclusions

References

Tables

Figures

◀

▶

◀

▶

Back

Close

Full Screen / Esc

Printer-friendly Version

Interactive Discussion



Aerosol extinction coefficients at ambient conditions

P. Zieger et al.

Title Page

Abstract

Introduction

Conclusions

References

Tables

Figures

◀

▶

◀

▶

Back

Close

Full Screen / Esc

Printer-friendly Version

Interactive Discussion



used to estimate $f(\text{RH})$. It will be shown that together with the measured size distribution and Mie theory this factor can be used to get an estimate of $f(\text{RH})$. The other parameters like the BC volume fraction $V_{\text{BC}}/V_{\text{tot}}$ or the coarse mode volume fraction $V_{\text{APS}}/V_{\text{tot}}$ show only low correlations with $f(\text{RH})$. The rather low correlation to $f(\text{RH})$ and the significant correlation to g can be explained by the fact that a larger coarse mode fraction is an indicator for the presence of sea salt, which exhibits a higher hygroscopic growth, while a larger BC fraction is an indicator for anthropogenic pollution with a reduced hygroscopic growth. This can also be seen in the significant anticorrelation of g vs. the BC volume fraction $V_{\text{BC}}/V_{\text{tot}}$: high amounts of BC in the aerosol reduce its ability for hygroscopic growth (Weingartner et al., 1997). The mean diameter $D_{\text{mean}} = N^{-1} \int_0^{\infty} (D_{\text{dry}} dN/d\log D_{\text{dry}}) d\log D_{\text{dry}}$ measured by the APS (representative for the coarse mode) and by the SMPS and APS (representative for the entire size distribution) show similar values of R^2 as the coarse mode fraction. The coarse mode proxies $V_{\text{APS}}/V_{\text{tot}}$ and D_{APS} are higher correlated to g than to $f(\text{RH})$, because the $f(\text{RH})$ is determined for the entire size distribution (where the hygroscopic properties may change with size) while g is representative for only one dry diameter. It may also point towards the effect that smaller but less hygroscopic particles may have a larger $f(\text{RH})$ than larger but more hygroscopic particles because of the non-linearity in the Mie-scattering. A similar effect was observed and modeled in Zieger et al. (2010) for Arctic aerosol which could also exhibit a large hygroscopic coarse mode due to sea salt. The scattering Ångström exponent α_{sp} (retrieved similar to Eq. (5) but using σ_{sp} instead of σ_{ap}) of the dry and wet (at $\text{RH} = 85\%$) scattering coefficient show no correlation with $f(\text{RH})$. α_{sp} is commonly used as a proxy for the mean size (as can be seen in the clear anticorrelation between α_{sp} and the volume coarse mode fraction $V_{\text{APS}}/V_{\text{tot}}$). This implies that they can not be used as a simple proxy for $f(\text{RH})$, as for example it has been proposed and verified for the typical aerosol found at the high alpine site Jungfraujoch (JFJ) (Nessler et al., 2005a; Fierz-Schmidhauser et al., 2010a). The reason for this is the possible presence of a hygroscopic coarse mode (sea salt) at Cabauw (and most probably for all measurement sites with maritime influence), whereas at the JFJ a

coarse mode is mainly composed of mineral dust with very low hygroscopicity. Neither the dry backscattering coefficient b_{dry} (measured by the nephelometer) nor the dry single scattering albedo $\omega_{0,\text{dry}}$ (e.g. measured by the nephelometer, the MAAP and/or the aethalometer) are suitable proxies. The Ångström exponent of the scattering enhancement factor $\alpha_{f(\text{RH})}$ shows no significant correlation to any in-situ parameters.

4.3 Closure study

To check for consistency within the aerosol in-situ measurements a closure study using Mie theory was performed. The main goal was to reproduce the WetNeph measurements using independent measurements of the hygroscopic growth factor (H-TDMA), the aerosol size distribution (SMPS and APS), the aerosol absorption (MAAP and aethalometer), and scattering properties (DryNeph). The Mie-based model is described in detail in Zieger et al. (2010). The focus was set on the period 4 July to 20 July 2009, because during this period all instruments were operating successfully (for the other periods the SMPS did not measure). Independent measurements of the chemical composition were not available for this study, but are needed to calculate the complex refractive index used in the Mie calculations. Therefore, an inversion of the dry scattering and absorption coefficients using the measured size distribution and Mie theory was done (assuming a 50×50 field of real and imaginary parts of the refractive index). This procedure is not a critical issue for the WetNeph closure itself because the closure will be done for a high RH (here, at 85%) as an example, where the particle's refractive index will be close to the one of water.

The retrieval of the refractive index showed additionally that the imaginary part anticorrelates well with the hygroscopic growth factor which is measured independently by the H-TDMA ($R^2 = 0.51$, see Fig. 4). This shows that less hygroscopic particles at Cabauw are also characterized by an enhanced absorption, which indicates the presence of black carbon. A functional description (e.g. polynomial fit) can not be established due to the clear and strong presence of organic matter at Cabauw (Morgan et al., 2010), which is expected to lower the hygroscopic growth and has a minor influence

Aerosol extinction coefficients at ambient conditions

P. Zieger et al.

Title Page

Abstract

Introduction

Conclusions

References

Tables

Figures

◀

▶

◀

▶

Back

Close

Full Screen / Esc

Printer-friendly Version

Interactive Discussion



on the refractive index (low absorption). Therefore, an extrapolation to $g = 1$ in order to estimate the imaginary part of BC can not be made without assumptions. The imaginary part versus the BC volume fraction showed a very good correlation ($R^2 = 0.96$, $m_i = 0.68V_{\text{BC}}/V_{\text{tot}} - 0.0013$ at 550 nm); an extrapolation to $V_{\text{BC}}/V_{\text{tot}} \rightarrow 1$ would lead to an imaginary part of pure BC of ~ 0.7 , which is in accordance with literature values (see e.g. Bond and Bergstrom, 2006). The good correlation is not surprising since the imaginary part was retrieved using the BC measurements from the MAAP next to the size distribution and nephelometer measurements.

The hygroscopic growth factor g is measured by the H-TDMA at the dry diameters of 35, 50, 75, 110, and 165 nm. Since the H-TDMA measured at a constant RH = 90%, the value of g for different RH was calculated using Eq. (2). The largest diameter is the most important one for the determination of the optical properties. The change of the size distribution at RH = 85% was calculated assuming that particles larger than 165 nm have the same hygroscopic growth as the 165-nm-particles. The result for the wet scattering coefficient $\sigma_{\text{sp}}(\text{RH} = 85\%)$ is presented in Fig. 5a (the results are shown for $\lambda = 550$ nm and are similar for the other nephelometer wavelengths). For the linear regression a bivariate weighted fit according to York et al. (2004) as described in Cantrell (2008) with the assumption of a 10% error in the measured (Anderson et al., 1996) and calculated scattering coefficients has been used. This method includes the uncertainties of both the x and y variables and allows the calculation of the uncertainties of the retrieved slope and intercept. The high correlation coefficient and the good linear relationship are clear indicators that the aerosol in-situ measurements are consistent with each other (at least for the investigated period). The slightly lower values of the calculated $\sigma_{\text{sp}}(\text{RH} = 85\%)$ can be explained by the fact that the H-TDMA measures only rather small particles and misses the coarse mode which might include large hygroscopic particles such as sea salt. This is also seen in the applied color code. While the H-TDMA measures particles with low hygroscopicity (e.g. $g < 1.3$, blue points) the measured values of $\sigma_{\text{sp}}(\text{RH} = 85\%)$ are larger than the calculated ones. One reason could be the presence of a mixture containing a polluted fine mode (e.g. soot) and a

Aerosol extinction coefficients at ambient conditions

P. Zieger et al.

Title Page

Abstract

Introduction

Conclusions

References

Tables

Figures

◀

▶

◀

▶

Back

Close

Full Screen / Esc

Printer-friendly Version

Interactive Discussion



coarse mode consisting of sea salt, which can not be measured with the H-TDMA. The calculated $f(\text{RH} = 85\%)$ using the measured g of the H-TDMA is therefore lower than that derived from the measurements (see Fig. 5b).

To further demonstrate this effect, the hygroscopic growth factor was derived via Mie theory from the WetNeph, DryNeph and size distribution measurements (for more details see Zieger et al. 2010). The results are presented in Fig. 6 together with the hygroscopic growth factors measured with the H-TDMA (both at $\text{RH} = 90\%$). While the correlation between both methods is quite good ($R^2 = 0.71$) and the agreement is good for certain periods, the WetNeph based g is generally slightly higher ($g_{\text{Mie}} = 1.3g_{\text{HTDMA}} - 0.4$ derived by an orthogonal linear regression), but there are certain periods where the differences increase substantially. These are most probably episodes with enhanced sea salt influence, as can be seen by an enlarged coarse mode measured by the APS and SMPS (see color code in Fig. 6).

The calculations were repeated using a fixed hygroscopic growth factor of $g(\text{RH} = 85\%) = 1.4$ (mean campaign value) to demonstrate the effect of assuming a constant hygroscopic growth. The result is depicted in Fig. 5c. The calculated $f(\text{RH})$ values are clearly lower than the measured values of $f(\text{RH})$. The color code shows the g measured by the H-TDMA, which is high for the underestimated and low for the overestimated values of $f(\text{RH})$.

If $f(\text{RH})$ needs to be predicted, the chemical composition (especially the coarse mode composition) needs to be known. Fierz-Schmidhauser et al. (2010a) and Nessler et al. (2005a) used one mean growth factor to successfully predict $f(\text{RH})$ at the JFJ, but they were in a comfortable position that the aerosol coarse mode consisted only of non-hygroscopic mineral dust.

The question arises whether other continuously measured aerosol properties can be used as a proxy to estimate $f(\text{RH})$ or g . $f(\text{RH})$ correlates poorly with other in-situ measured parameters as already shown in Fig. 3, but clearly correlates with g . g on the other hand correlates well with the coarse mode and black carbon volume fraction. An empirical equation was retrieved from the available measurements

Aerosol extinction coefficients at ambient conditions

P. Zieger et al.

Title Page

Abstract

Introduction

Conclusions

References

Tables

Figures

⏪

⏩

◀

▶

Back

Close

Full Screen / Esc

Printer-friendly Version

Interactive Discussion



($g(\text{RH} = 85\%) = b_1 + b_2 V_{\text{BC}}/V_{\text{tot}} + b_3 V_{\text{APS}}/V_{\text{tot}} + b_4 V_{\text{APS}}/V_{\text{tot}} \cdot V_{\text{BC}}/V_{\text{tot}}$ with $b_1 = 1.38$, $b_2 = -1.64$, $b_3 = 0.35$, and $b_4 = -1.77$) and found to be the best suitable equation. The result of the $f(\text{RH})$ calculation compared to the measurements is presented in Fig. 5d. Although the variation is quite large, an improvement compared to the constant chemistry assumption is clearly seen. Nevertheless, these examples demonstrate the need for a full chemical analysis and measured size distribution to predict $f(\text{RH})$ if no humidified nephelometer (or at least H-TDMA) measurements are available.

4.4 Comparison to remote sensing data

The WetNeph measurements allow the determination of the ambient extinction coefficient, assuming that the absorption coefficient does not change with RH. This assumption can be made, because the scattering is the dominant part of the extinction (median $\omega_0 = 0.81$, 10th perc. $\omega_0 = 0.70$, 90th perc. $\omega_0 = 0.89$ at dry conditions for the entire campaign) and model studies for free tropospheric aerosol (although with a higher ω_0) show that the effect of RH on the absorption coefficient (with respect to the extinction) is negligible (Nessler et al., 2005b). The extinction is then calculated as follows:

$$\sigma_{\text{ep}}(\text{RH}) = c_p (f(\text{RH})\sigma_{\text{sp}} + \sigma_{\text{ap}}). \quad (9)$$

σ_{sp} and σ_{ap} are measured by the DryNeph and the MAAP and aethalometer under dry conditions. c_p is a correction factor for pressure and temperature differences (see below). All optical measurements were inter- or extrapolated to the relevant wavelength using the Ångström law (Eq. 5, with σ_{ep}). $\alpha_{\text{ap}} = 0.84$ was assumed for periods without aethalometer measurements which represents the mean value measured until the 6th of July by the aethalometer at the site. $f(\text{RH})$ was interpolated assuming a linear relationship. Time periods with $\text{RH} > 95\%$ were ignored, due to the uncertainty in the parameterization of $f(\text{RH})$ at very high RH values (e.g. $f(\text{RH}) \rightarrow \infty$ for $\text{RH} \rightarrow 100\%$). $c_p = \rho(h)T_0/\rho_0T(h)$ accounts for pressure and temperature differences inside (ρ_0 , T_0) and outside ($\rho(h)$, $T(h)$) the nephelometer. For the calculation of $\rho(h)$

29705

Aerosol extinction coefficients at ambient conditions

P. Zieger et al.

Title Page

Abstract

Introduction

Conclusions

References

Tables

Figures

◀

▶

◀

▶

Back

Close

Full Screen / Esc

Printer-friendly Version

Interactive Discussion



the barometric formula was used, whereas h is the height of the RH measurement. This is mainly of importance for the comparison to the MPI measurements where the measured extinction coefficient is a mean value for a varying layer height (20–5000 m). At the Cabauw tower, the temperature and dew point (from which the RH can be derived via the Magnus formula) are continuously measured at 10, 20, 40, 80, 140, and 200 m. For the MPI comparison the temperature and RH profiles were taken from the operational weather forecast model COSMO (based on assimilated data, see <http://www.cosmo-model.org/>). It was assumed that the aerosol type and concentration are constant with altitude and only RH is changing. Only the retrievals at the lowest height level of the remote sensing instruments were compared to in-situ measurements.

4.4.1 MAX-DOAS

For comparison with the in-situ measurements, aerosol extinction coefficient from the lowermost layer of the MAX-DOAS profiles from BIRA, IUPHD and JAMSTEC are used, whereas a mean aerosol extinction coefficient in the boundary layer is estimated from the MPI data by retrieving the layer height and the aerosol optical thickness. BIRA and IUPHD retrievals use a layer thickness of 200 m, whereas from the JAMSTEC retrieval with a layer height of 1 km, an extinction coefficient representative for the lowermost 200 m has been estimated by assuming an exponentially decreasing extinction profile. The $f(\text{RH})$ value was calculated for each available RH measurements of the tower (for MPI taken from the COSMO model), and a mean value was then calculated using Eq. (9). For the correction factor c_p , the pressure was taken from ground based measurements (and taking the barometric height formula for the height dependency) and the temperature was measured next to the RH sensors (for MPI again the COSMO data was used).

In Fig. 7 an example measurement of 24 June 2009 is seen. This day was characterized by almost entirely cloud free conditions in the morning and was classified as one of the golden days during CINDI (Roscoe et al., 2010). This is also reflected

Aerosol extinction coefficients at ambient conditions

P. Zieger et al.

Title Page

Abstract

Introduction

Conclusions

References

Tables

Figures

⏪

⏩

◀

▶

Back

Close

Full Screen / Esc

Printer-friendly Version

Interactive Discussion



in the lidar measurement (Fig. 7a), which showed the appearance of cirrus clouds at around 10 a.m. and low level clouds at around 11:30 a.m. The agreement between MAX-DOAS and in-situ is good during the forenoon, which was characterized by high ambient RH values, which were decreasing until noon (see color code of ambient in-situ values in Fig. 7b–e); concurrently the extinction was decreasing within all measurements. From approx. 10:30 a.m. (12 a.m. for IUPHD) the MAX-DOAS and ambient in-situ values of σ_{ep} were diverging. This was coincident with an increase of the planetary boundary layer height and the appearance of low level clouds (see lidar measurement in Fig. 7a), while the surface values of RH (between 0–200 m) stayed below 70%. The comparison of the aerosol optical depth (AOD), which is the integral of σ_{ep} over the vertical column, retrieved by the MAX-DOAS and measured by a Cimel sun photometer showed good agreement during the entire day, although this is just a columnar value being compared giving no information on the true profile shape (further details in Frieß et al., 2010).

Figures 8 and 9 displays the comparison of the entire data set. All MAX-DOAS instruments detect generally a higher extinction coefficient than the in-situ measurements. The slope of the applied bivariate linear regression (Cantrell, 2008; York et al., 2004) varies from 2.9 (IUPHD), 3.4 (JAMSTEC) to 3.4 (BIRA, with sun photometer (Cimel) used as input values). The MPI MAX-DOAS shows a lower slope (1.5), but has to be treated with care since the retrieval height varied and RH profiles were taken from a re-analyzed weather model (COSMO). All comparisons are well correlated ($R^2 = 0.62$ to 0.78). An overview of the coefficients retrieved from the orthogonal linear fit and the correlation is found in Table 2. Slope and R^2 improve slightly if only identical time periods (when all four MAX-DOAS instruments were measuring at the same time) are being compared, although the number of comparable points is largely reduced (see Table 2). A distinct number of points show a good agreement and are located on the 1:1-line. The color code in Fig. 8 reveals that these are times with a low aerosol optical depth (data from the AERONET sun photometer measurement, level 2.0). Figure 9 shows the same comparison, but with the planetary boundary layer (PBL) height as

Aerosol extinction coefficients at ambient conditions

P. Zieger et al.

Title Page

Abstract

Introduction

Conclusions

References

Tables

Figures

◀

▶

◀

▶

Back

Close

Full Screen / Esc

Printer-friendly Version

Interactive Discussion



color code. The PBL height is measured by a ceilometer (Vaisala, Model LD-40; for details concerning the algorithm see de Haij et al., 2007, 2010). The points with better agreement show a low PBL height.

Figure 10 illustrates the comparison of the MPI measurement, where the layer height is kept variable during the retrieval. The agreement improves with decreasing layer height despite the assumptions that had to be made (well mixed aerosol layer, same aerosol type, RH from COSMO).

The error bars of the ambient in-situ extinction coefficient in Figs. 7–10 were derived from Gaussian error propagation assuming a 10% uncertainty of the nephelometer (Anderson et al., 1996) and a 12% uncertainty of the MAAP (Petzold and Schönlinner, 2004).

For the BIRA and IUPHD retrieval the error bars represent the sum of the noise and smoothing error. Forward model errors were not considered here (Rodgers, 2000; Frieß et al., 2006; Clémer et al., 2010). For the JAMSTEC retrieval the errors have been quantified by the retrieval covariance matrix, which is defined to represent the sum of the smoothing error and the retrieval noise error (Rodgers, 2000). For the MPI retrieval so far no full error assessment was implemented, and the errors were assumed to be $0.25\sigma_{ep} + 0.05 \times 10^{-3} \text{ m}^{-1}$.

As already mentioned, BIRA uses the values of the asymmetry factor and the single scattering albedo inverted from sun photometer measurements in their standard retrieval. The comparison improves if in-situ measurements (at ambient conditions) of the asymmetry factor and the single scattering albedo are taken as input parameters (see Table 2).

The following hypotheses concerning the disagreement are being made. On the in-situ side:

- Particle losses due to impaction or diffusion in the inlet system
- Underestimation of the measured extinction due to the PM_{10} size cut
- Parameterization of $f(\text{RH})$ (Eq. (3), large errors for $\text{RH} > 90\%$)

29708

Aerosol extinction coefficients at ambient conditions

P. Zieger et al.

Title Page

Abstract

Introduction

Conclusions

References

Tables

Figures

◀

▶

◀

▶

Back

Close

Full Screen / Esc

Printer-friendly Version

Interactive Discussion



4.4.2 LIDAR

Due to the intensive data processing and long averaging times, only 22 profiles (within the period 23 June–20 September) of the aerosol extinction coefficient measured by the CAELI lidar could be compared to the in-situ measurements. The aerosol extinction coefficient (at 355 nm) can be measured directly using the Raman channel above approx. 750 m. The backscatter signal starts at approx. 70 m and can be used to extrapolate the direct measurement of σ_{ep} if an appropriate lidar ratio LR (Eq. 7) is assumed. Instead of an educated guess, the measured LR of the upper layers between 700 and 1700 m was determined (mean values for 200 m thick levels) and multiplied with the backscatter signal.

An example day is presented in Fig. 11. The extinction is directly measured above 750 m (black line). The LR of the upper layers increase with height from LR = 37 to LR = 48 (probably due to changing RH or/and aerosol type changes or lower signal to noise ratio). These values are used to calculate σ_{ep} from the backscatter signal. The in-situ values at dry (black square) and at ambient conditions at the RH measurement of the tower (color coded circles) are also shown. The large RH gradient results in a strong increase of σ_{ep} concurrently measured by the in-situ and the lidar.

A comparison of all lidar to in-situ measurements is shown in Fig. 12. Only LR > 0 were considered for reasonable extrapolations. The LR from the lowest possible layer is separately highlighted (colored square or circle). An orthogonal linear regression (without weights) revealed that the lidar retrieved about 1.8 higher extinction coefficients compared to the ambient in-situ values. Both measurements are well correlated ($R^2 = 0.79$). Nighttime measurements showed a much better agreement (slope 1.2, $R^2 = 0.93$) compared to daytime measurements, which might be due to lower noise in the lidar measurements during nighttime.

Aerosol extinction coefficients at ambient conditions

P. Zieger et al.

Title Page

Abstract

Introduction

Conclusions

References

Tables

Figures

◀

▶

◀

▶

Back

Close

Full Screen / Esc

Printer-friendly Version

Interactive Discussion



5 Conclusions

In this study, the influence of water uptake on the aerosol extinction coefficient was investigated during a 4-months campaign at the Cabauw field station (The Netherlands) using direct measurements of aerosol optical and micro-physical properties. While the scattering coefficient was measured as a function of RH, the absorption coefficient was measured dry and assumed not to change with RH. The scattering enhancement factor $f(\text{RH})$ was found to be highly variable ($f(\text{RH})$ varied between ~ 1.4 and 3.8 at $\text{RH} = 85\%$) and dependent on the air mass origin. Continental aerosol showed a lower scattering enhancement possibly due to anthropogenic pollution and lower sea salt content. Hysteresis was observed only during some very events, when the air masses arrived directly from the oceans. The main quantity to estimate $f(\text{RH})$ from other continuous in-situ measurements was found to be the hygroscopic growth factor measured e.g. by a H-TDMA or derived from chemical composition measurements. The use of the scattering Ångström exponent did not provide favorable results, due to the large variability in the chemical composition. This makes a simple prediction of $f(\text{RH})$ at Cabauw, especially in contrast to other sites (e.g. Jungfraujoch), quite difficult. Here, continuous measurements of $f(\text{RH})$ and/or better chemical composition measurements would be desirable to better relate dry measured values to the ambient ones. A closure study, which relied on the measured size distribution and the hygroscopic growth, showed the consistency of the aerosol in-situ measurements. The imaginary part of the retrieved complex refractive index was found to correlate well with the hygroscopic growth factor of the HTDMA, which means that more absorbing particles grow less. As a proof of concept, the in-situ measurements were compared with remote sensing data from MAX-DOAS and lidar measurements. Good correlation was found between in-situ and MAX-DOAS measurements. For certain cases (low AOD and low PBL height) good agreement was found, but for most of the time MAX-DOAS retrieved a ~ 1.5 – 3.4 higher extinction coefficient. Differences could have been caused by e.g. particle losses in the inlet system (all remote-sensing instruments were measuring generally higher

Aerosol extinction coefficients at ambient conditions

P. Zieger et al.

Title Page

Abstract

Introduction

Conclusions

References

Tables

Figures

◀

▶

◀

▶

Back

Close

Full Screen / Esc

Printer-friendly Version

Interactive Discussion



extinction) or by the fact that the limited vertical resolution of the MAX-DOAS retrieval overestimated the extinction in the lowest layer when lofted layers were present. In addition, the MAX-DOAS retrieval could have been influenced by the horizontal aerosol gradient, which could have exhibited large variations. The smaller slope of the regression line for the MPI measurements could indicate that the coarser resolution with more simplified assumptions is a more robust MAX-DOAS aerosol retrieval. Lidar and in-situ comparison found to be in better agreement, although the direct measurement of the ambient extinction coefficient started from an altitude above 750 m. Extrapolation with the backscatter signal showed a good correlation ($R^2 = 0.79$) and a higher extinction compared to in-situ (slope of 1.81), which improved (slope of 1.14, $R^2 = 0.93$) if only nighttime measurements were compared.

Acknowledgements. We thank Jacques Warmer and the staff of KNMI at the CESAR site for providing an excellent service during our campaign. We thank the CINDI local organization team at KNMI, in particular Ankie Piters, Mark Kroon, and Jennifer Hains, for facilitating this very successful campaign. We gratefully acknowledge Henk Klein-Baltink (KNMI) for providing the ceilometer data. We also gratefully acknowledge the easy access of the meteorological data used in this work via <http://www.cesar-observatory.nl>. We thank Rahel Fierz (PSI) for valuable discussions. Many thanks to Michel Tinquely (PSI) for helping out with the COSMO data, which was provided by the Swiss Federal Office of Meteorology and Climatology (MeteoSwiss). NILU is gratefully acknowledged for providing the air mass trajectories. Many thanks to A. Rozanov from the Institute of Environmental Physics, University of Bremen, for providing the SCIATRAN radiative transfer model to IUPHD. Hitoshi Irie thanks H. Takashima, Y. Kanaya, and PREDE, Co., Ltd for their technical assistance in developing and operating the MAX-DOAS instrument. Observation by JAMSTEC was supported by the Japan EOS Promotion Program of the Ministry of Education, Culture, Sports, Science and Technology (MEXT), and by the Global Environment Research Fund (S-7) of the Japanese Ministry of the Environment. Katrijn Clémer (BIRA-IASB) was financially supported by the AGACC project (contract SD/AT/10A) funded by the Belgian Federal Science Policy Office. This work was financially supported by the ESA Climate Change Initiative Aerosol_cci (ESRIN/Contract No. 4000101545/10/I-AM) and by the EC-projects: Global Earth Observation and Monitoring (GEOmon, contract 036677) and European Supersites for Atmospheric Aerosol Research (EUSAAR, contract 026140).

Aerosol extinction coefficients at ambient conditions

P. Zieger et al.

Title Page

Abstract

Introduction

Conclusions

References

Tables

Figures

◀

▶

◀

▶

Back

Close

Full Screen / Esc

Printer-friendly Version

Interactive Discussion



References

- Ackermann, J.: The extinction-to-backscatter ratio of tropospheric aerosols: a numerical study, *J. Atmos. Ocean. Tech.*, 15, 1043–1050, 1998. 29697
- Anderson, T., Covert, D., Marshall, S., Laucks, M., Charlson, R., Waggoner, A., Ogren, J.,
5 Caldwell, R., Holm, R., Quant, F., Sem, G., Wiedensohler, A., Ahlquist, N., and Bates, T.:
Performance characteristics of a high-sensitivity, three-wavelength, total scatter/backscatter
nephelometer, *J. Atmos. Oceanic Technol.*, 13, 967–986, 1996. 29691, 29703, 29708
- Ansmann, A., Wandinger, U., Riebesell, M., Weitkamp, C., and Michaelis, W.: Independent
10 measurement of extinction and backscatter profiles in cirrus clouds by using a combined
Raman elastic-backscatter lidar, *Appl. Opt.*, 31, 7113–7113, 1992. 29696, 29697
- Apituley, A., Wilson, K.M., Potma, C., Volten, H., and de Graaf, M.: Performance Assessment
and Application of Caeli – A high-performance Raman lidar for diurnal profiling of Water
Vapour, Aerosols and Clouds, Proceedings of the 8th International Symposium on Tropo-
spheric Profiling, 19–23 October 2009, Delft, The Netherlands, 2009. 29696
- 15 Birmili, W., Stopfkuchen, K., Hermann, M., Wiedensohler, A., and Heintzenberg, J.: Particle
penetration through a 300 m inlet pipe for sampling atmospheric aerosols from a tall meteo-
rological tower, *Aerosol Sci. Technol.*, 41, 811–817, 2007. 29690
- Bond, T. C. and Bergstrom, R. W.: Light absorption by carbonaceous particles: an investigative
review, *Aerosol Sci. Technol.*, 40(1), 27–67, 2006. 29703
- 20 Cantrell, C. A.: Technical Note: Review of methods for linear least-squares fitting of data
and application to atmospheric chemistry problems, *Atmos. Chem. Phys.*, 8, 5477–5487,
doi:10.5194/acp-8-5477-2008, 2008. 29703, 29707
- Carrico, C. M., Kus, P., Rood, M. J., Quinn, P. K., and Bates, T. S.: Mixtures of pollution, dust,
sea salt, and volcanic aerosol during ACE-Asia: radiative properties as a function of relative
25 humidity, *J. Geophys. Res.*, 108(D23), 8650, doi:10.1029/2003JD003405, 2003. 29687,
29698
- Clarke, A. D., Howell, S., Quinn, P. K., Bates, T. S., Ogren J. A., Andrews, E., Jefferson, A.,
Massling, A., Mayol-Bracero, O., Maring, H., Savoie, D., and Cass, G.: INDOEX aerosol:
A comparison and summary of chemical, microphysical, and optical properties observed
30 from land, ship, and aircraft, *J. Geophys. Res.*, 107, 8033, doi:803310.1029/2001JD000572,
2002. 29698
- Clémer, K., Van Roozendaal, M., Fayt, C., Hendrick, F., Hermans, C., Pinardi, G., Spurr, R.,

Aerosol extinction coefficients at ambient conditions

P. Zieger et al.

Title Page

Abstract

Introduction

Conclusions

References

Tables

Figures

◀

▶

◀

▶

Back

Close

Full Screen / Esc

Printer-friendly Version

Interactive Discussion



Aerosol extinction coefficients at ambient conditions

P. Zieger et al.

Title Page

Abstract

Introduction

Conclusions

References

Tables

Figures

◀

▶

◀

▶

Back

Close

Full Screen / Esc

Printer-friendly Version

Interactive Discussion



Wang, P., and De Mazière, M.: Multiple wavelength retrieval of tropospheric aerosol optical properties from MAXDOAS measurements in Beijing, *Atmos. Meas. Tech.*, 3, 863–878, doi:10.5194/amt-3-863-2010, 2010. 29695, 29696, 29708, 29721

Collaud Coen, M., Weingartner, E., Apituley, A., Ceburnis, D., Fierz-Schmidhauser, R., Flen-
tje, H., Henzing, J. S., Jennings, S. G., Moerman, M., Petzold, A., Schmid, O., and Bal-
tensperger, U.: Minimizing light absorption measurement artifacts of the Aethalometer: eval-
uation of five correction algorithms, *Atmos. Meas. Tech.*, 3, 457–474, doi:10.5194/amt-3-
457-2010, 2010. 29692

de Haij, M., Klein Baltink, H., and Wauben, W.: Continuous mixing layer height determination
using the LD40-ceilometer: a feasibility study, KNMI Scientific Report WR 2007-01, De Bilt,
The Netherlands, 2007. 29708

de Haij, M., Wauben, W., Klein Baltink, H., and Apituley, A.: Determination of the mixing layer
height by a ceilometer, Proceedings of the 8th International Symposium on Tropospheric
Profiling, 19–23 October, Delft, The Netherlands, edited by: Apituley, A., Russchenberg, H.
W. J., Monna, W. A. A., ISBN 978-90-6960-233-2, 2010. 29708

Deutschmann, T. and Wagner, T.: TRACY-II Users manual, [http://joseba.mpch-mainz.mpg.de/
Strahlungstransport.htm](http://joseba.mpch-mainz.mpg.de/Strahlungstransport.htm), 2008. 29721

Ehn, M., Petäjä, T., Aufmhoff, H., Aalto, P., Hämeri, K., Arnold, F., Laaksonen, A., and Kul-
mala, M.: Hygroscopic properties of ultrafine aerosol particles in the boreal forest: diurn-
al variation, solubility and the influence of sulfuric acid, *Atmos. Chem. Phys.*, 7, 211–222,
doi:10.5194/acp-7-211-2007, 2007. 29693

Ferrare, R. A., Melfi, S. H., Whiteman, D. N., Evans, K. D., and Leifer, R.: Raman lidar measure-
ments of aerosol extinction and backscattering, 1. Methods and comparisons, *J. Geophys.
Res.*, 103(D16), 19663–19672, 1998. 29687

Fierz-Schmidhauser, R., Zieger, P., Gysel, M., Kammermann, L., DeCarlo, P. F., Bal-
tensperger, U., and Weingartner, E.: Measured and predicted aerosol light scattering en-
hancement factors at the high alpine site Jungfraujoch, *Atmos. Chem. Phys.*, 10, 2319–2333,
doi:10.5194/acp-10-2319-2010, 2010, 2010a. 29687, 29701, 29704

Fierz-Schmidhauser, R., Zieger, P., Vaishya, A., Monahan, C., Bialek, J., O'Dowd, C.D., Jen-
nings, S. G., Baltensperger, U., and Weingartner, E.: Light scattering enhancement fac-
tors in the marine boundary layer (Mace Head, Ireland), *J. Geophys. Res.*, 115, D20204,
doi:10.1029/2009JD013755, 2010b. 29687

Fierz-Schmidhauser, R., Zieger, P., Wehrle, G., Jefferson, A., Ogren, J. A., Baltensperger,

Aerosol extinction coefficients at ambient conditions

P. Zieger et al.

[Title Page](#)[Abstract](#)[Introduction](#)[Conclusions](#)[References](#)[Tables](#)[Figures](#)[◀](#)[▶](#)[◀](#)[▶](#)[Back](#)[Close](#)[Full Screen / Esc](#)[Printer-friendly Version](#)[Interactive Discussion](#)

- U., and Weingartner, E.: Measurement of relative humidity dependent light scattering of aerosols, *Atmos. Meas. Tech.*, 3, 39–50, doi:10.5194/amt-3-39-2010, 2010c. 29690
- Fitzgerald, J. W., Hoppel, W. A., and Vietti, M. A.: The size and scattering coefficient of urban aerosol particles at Washington, DC as a function of relative humidity, *J. Atmos. Sci.*, 39, 1838–1852, 1982. 29687
- 5 Freudenthaler, V.: The Telecover Test: A quality assurance tool for the optical part of a lidar system, <http://www.meteo.physik.uni-muenchen.de/~st212fre/ILRC24/index.html>, Proc. of the 24th ILRC, Boulder, Colorado, 23–27 June 2008. 29697
- Frieß, U., Monks, P. S., Remedios, J. J., Rozanov, A., Sinreich, R., Wagner, T., and Platt, U.: MAX-DOAS O₄ measurements: A new technique to derive information on atmospheric aerosols: 2. Modeling studies, *J. Geophys. Res.*, 111, D14203, doi:10.1029/2005JD006618, 2006. 29694, 29695, 29708, 29721
- 10 Frieß, U., Clémer, K., Irie, H., Vlemmix, T., Wagner, T., Wittrock, F., Yilmaz, S., Zieger, P., and Apituley, A.: Intercomparison of MAX-DOAS aerosol profile retrieval algorithms during the CINDI campaign, *Atmos. Meas. Tech. Discuss.*, in preparation, 2010. 29688, 29696, 29707
- Gysel, M., McFiggans, G., and Coe, H.: Inversion of tandem differential mobility analyser (TDMA) measurements, *J. Aerosol Sci.*, 40, 134–151, doi:10.1016/j.jaerosci.2008.07.013, 2008. 29694
- 15 Heckel, A., Richter, A., Tarsu, T., Wittrock, F., Hak, C., Pundt, I., Junkermann, W., and Burrows, J. P.: MAX-DOAS measurements of formaldehyde in the Po-Valley, *Atmos. Chem. Phys.*, 5, 909–918, doi:10.5194/acp-5-909-2005, 2005. 29694
- Hess, M. P., Koepke, P., and Schultz, I.: Optical properties of aerosols and clouds: The software package OPAC, *Bull. Meteorol. Soc.*, 79, 831–844, 1998. 29721
- Holben, B. N., Eck, T. F., Slutsker, I., Tanre, D., Buis, J. P., Setzer, A., Vermote, E., Reagan, J. A., Kaufman, Y. J., Nakajima, T., Lavenu, F., Jankowiak, I., and Smimov, A.: AERONET - A federated instrument network and data archive for aerosol characterization, *Rem. Sens. Env.*, 66(1), 1–16, 1998. 29721
- 20 Hönninger, G. and Platt, U.: Observations of BrO and its vertical distribution during surface ozone depletion at Alert, *Atmos. Environ.*, 36, 2481–2490, 2002. 29694
- Hönninger, G., von Friedeburg, C., and Platt, U.: Multi axis differential optical absorption spectroscopy (MAX-DOAS), *Atmos. Chem. Phys.*, 4, 231–254, doi:10.5194/acp-4-231-2004, 2004. 29694
- 30 Irie, H., Kanaya, Y., Akimoto, H., Iwabuchi, H., Shimizu, A., and Aoki, K.: First retrieval of

tropospheric aerosol profiles using MAX-DOAS and comparison with lidar and sky radiometer measurements, *Atmos. Chem. Phys.*, 8, 341–350, doi:10.5194/acp-8-341-2008, 2008. 29694, 29721

Irie, H., Kanaya, Y., Akimoto, H., Iwabuchi, H., Shimizu, A., and Aoki, K.: Dual-wavelength aerosol vertical profile measurements by MAX-DOAS at Tsukuba, Japan, *Atmos. Chem. Phys.*, 9, 2741–2749, doi:10.5194/acp-9-2741-2009, 2009. 29721

Iwabuchi, H.: Efficient Monte Carlo methods for radiative transfer modeling, *J. Atmos. Sci.*, 63(9), 2324–2339, 2006. 29721

Köhler, H.: The nucleus and growth of hygroscopic droplets, *T. Faraday Soc.*, 32, 1152–1161, 1936. 29686

Kotchenruther, R. A. and Hobbs, P. V.: Humidification factors of aerosols from biomass burning in Brazil, *J. Geophys. Res.*, 103(D24), 32081–32089, 1998. 29687

Leser, H., Hönninger, G., and Platt, U.: MAX-DOAS measurements of BrO and NO₂ in the marine boundary layer, *Geophys. Res. Lett.*, 30(10), 1537, doi:10.1029/2002GL015811, 2003. 29694

Li, X., Brauers, T., Shao, M., Garland, R. M., Wagner, T., Deutschmann, T., and Wahner, A.: MAX-DOAS measurements in southern China: retrieval of aerosol extinctions and validation using ground-based in-situ data, *Atmos. Chem. Phys.*, 10, 2079–2089, doi:10.5194/acp-10-2079-2010, 2010. 29688, 29695, 29721

Liu, B. Y. H., Pui, D. Y. H., Whitby, K. T., Kittelson, D. B., Kousaka, Y., and McKenzie, R. L.: Aerosol mobility chromatograph – new detector for sulfuric-acid aerosols, *Atmos. Environ.*, 12, 99–104, 1978. 29693

Ming, Y. and Russell, L.: Predicted hygroscopic growth of sea salt aerosol, *J. Geophys. Res.*, 106(D22), 28259–28274, 2001. 29700

Morgan, W. T., Allan, J. D., Bower, K. N., Esselborn, M., Harris, B., Henzing, J. S., Highwood, E. J., Kiendler-Scharr, A., McMeeking, G. R., Mensah, A. A., Northway, M. J., Osborne, S., Williams, P. I., Krejci, R., and Coe, H.: Enhancement of the aerosol direct radiative effect by semi-volatile aerosol components: airborne measurements in North-Western Europe, *Atmos. Chem. Phys.*, 10, 8151–8171, doi:10.5194/acp-10-8151-2010, 2010. 29688, 29702

Müller, T., Henzing, J. S., de Leeuw, G., Wiedensohler, A., Alastuey, A., Angelov, H., Bizjak, M., Collaud Coen, M., Engström, J. E., Gruening, C., Hillamo, R., Hoffer, A., Imre, K., Ivanow, P., Jennings, G., Sun, J. Y., Kalivitis, N., Karlsson, H., Komppula, M., Laj, P., Li, S.-M., Lunder, C., Marinoni, A., Martins dos Santos, S., Moerman, M., Nowak, A., Ogren, J. A., Petzold,

Aerosol extinction coefficients at ambient conditions

P. Zieger et al.

Title Page

Abstract

Introduction

Conclusions

References

Tables

Figures

◀

▶

◀

▶

Back

Close

Full Screen / Esc

Printer-friendly Version

Interactive Discussion



Aerosol extinction coefficients at ambient conditions

P. Zieger et al.

Title Page

Abstract

Introduction

Conclusions

References

Tables

Figures

◀

▶

◀

▶

Back

Close

Full Screen / Esc

Printer-friendly Version

Interactive Discussion



A., Pichon, J. M., Rodriguez, S., Sharma, S., Sheridan, P. J., Teinilä, K., Tuch, T., Viana, M., Virkkula, A., Weingartner, E., Wilhelm, R., and Wang, Y. Q.: Characterization and intercomparison of aerosol absorption photometers: result of two intercomparison workshops, *Atmos. Meas. Tech. Discuss.*, 3, 1511–1582, doi:10.5194/amtd-3-1511-2010, 2010. 29691

5 Nessler, R., Weingartner, E., and Baltensperger, U.: Adaptation of dry nephelometer measurements to ambient conditions at the Jungfraujoch, *Environ. Sci. Technol.*, 39, 2219–2228, 2005a. 29687, 29701, 29704

Nessler, R., Weingartner, E., and Baltensperger, U.: Effect of humidity on aerosol light absorption and its implications for extinction and the single scattering albedo illustrated for a site in the lower free troposphere, *J. Aerosol Sci.*, 36, 958–972, 2005b. 29705

10 Petters, M. D. and Kreidenweis, S. M.: A single parameter representation of hygroscopic growth and cloud condensation nucleus activity, *Atmos. Chem. Phys.*, 7, 1961–1971, doi:10.5194/acp-7-1961-2007, 2007. 29687

Petzold, A. and Schönlinner, M.: Multi-angle absorption photometry – a new method for the measurement of aerosol light absorption and atmospheric black carbon, *J. Aerosol Sci.*, 35, 421–441, 2004. 29691, 29708

15 Philippin, S., Laj, P., Putaud, J.-P., Wiedensohler, A., de Leeuw, G., Fjaeraa, A.M., Platt, U., Baltensperger, U., Fiebig, M.: EUSAAR - An Unprecedented Network of Aerosol Observation in Europe. *Eurozoru Kenkyu, JAAST*, 24(2), 78–83, 2009. 29689

20 Piters, A., Hains, J., Boersma, F., Kroon, M., Wittrock, F., van Roozendaal, M., et al.: The Cabauw Intercomparison campaign for Nitrogen Dioxide Measuring Instruments (CINDI), June/July 2009, The Netherlands, *Atmos. Meas. Tech. Discuss.*, in preparation, 2010. 29689

Platt, U. and Stutz, J.: *Differential Optical Absorption Spectroscopy: Principles and Applications*, Springer-Verlag, Berlin, 2008. 29694

25 Rodgers, C. D.: *Inverse Methods for Atmospheric Sounding: Theory and Practice*, Ser. Atmos. Oceanic Planet. Phys., vol. 2, F.W. Taylor, World Sci., Hackensack, N.Y., 2000. 29695, 29708

Roscoe, H. K., Van Roozendaal, M., Fayt, C., du Piesanie, A., Abuhassan, N., Adams, C., Akrami, M., Cede, A., Chong, J., Clmer, K., Friess, U., Gil Ojeda, M., Goutail, F., Graves, R., Griesfeller, A., Grossmann, K., Hemerijckx, G., Hendrick, F., Herman, J., Hermans, C., Irie, H., Johnston, P. V., Kanaya, Y., Kreher, K., Leigh, R., Merlaud, A., Mount, G. H., Navarro, M., Oetjen, H., Pazmino, A., Perez-Camacho, M., Peters, E., Pinardi, G., Puentedura, O., Richter, A., Schnhardt, A., Shaiganfar, R., Spinei, E., Strong, K., Takashima, H., Vlemmix, T., Vrekoussis, M., Wagner, T., Wittrock, F., Yela, M., Yilmaz, S., Boersma, F., Hains, J.,

Aerosol extinction coefficients at ambient conditions

P. Zieger et al.

Title Page

Abstract

Introduction

Conclusions

References

Tables

Figures

◀

▶

◀

▶

Back

Close

Full Screen / Esc

Printer-friendly Version

Interactive Discussion



Kroon, M., Piters, A., and Kim, Y. J.: Intercomparison of slant column measurements of NO₂ and O₄ by MAX-DOAS and zenith-sky UV and visible spectrometers, *Atmos. Meas. Tech.*, 3, 1629–1646, doi:10.5194/amt-3-1629-2010, 2010. 29689, 29695, 29696, 29706

Rozanov, A., Rozanov, V., and Burrows, J. P.: A numerical radiative transfer model for a spherical planetary atmosphere: combined differential-integral approach involving the Picard iterative approximation, *J. Quant. Spec. Rad. Trans.*, 69, 491–512, 2001. 29721

Russchenberg, H. W. J., Bosveld, F., Swart, D. P. J., ten Brink, H., de Leeuw, G., Uijlenhoet, R., Arbesser-Rastburg, B., van der Marel, H., Ligthart, L., Boers, R., and Apituley, A.: Ground-based atmospheric remote sensing in The Netherlands; European outlook, *IEICE Transactions on Communications*, E88-B(6), 2252–2258, doi:10.1093/ietcom/e88-b.6.2252, 2005. 29688

Salemink, H. W. M., Schotanus, P., and Bergwerff, J. B.: Quantitative lidar at 532 nm for vertical extinction profiles and the effect of relative humidity, *Appl. Phys.*, 34, 187–189, 1984. 29697

Sheridan, P. J., Delene, D. J., and Ogren, J. A.: Four years of continuous surface aerosol measurements from the Department of Energy's Atmospheric Radiation Program Southern Great Plains Cloud and Radiation Testbed site, *J. Geophys. Res.*, 106, 20735–20747, 2001. 29687

Sinreich, R., Frieß, U., Wagner, T., and Platt, U.: Multi axis differential optical absorption spectroscopy (MAX-DOAS) of gas and aerosol distributions, *Faraday Discuss.*, 130, 153–164, doi:10.1039/b419274, 2005. 29694

Sjogren, S., Gysel, M., Weingartner, E., Baltensperger, U., Cubison, M. J., Coe, H., Zardini, A. A., Marcolli, C., Krieger, U. K., and Peter, T.: Hygroscopic growth and water uptake kinetics of two-phase aerosol particles consisting of ammonium sulfate, adipic and humic acid mixtures, *J. Aerosol Sci.*, 38, 157–171, 2007. 29691

Spurr, R.: LIDORT and VLIDORT: Linearized pseudo-spherical scalar and vector discrete ordinate radiative transfer models for use in remote sensing retrieval problems, *Light Scattering Reviews*, Volume 3, edited by: Kokhanovsky, A., Springer, 2008. 29721

Stohl, A. and Seibert, P.: Accuracy of trajectories as determined from the conservation of meteorological tracers, *Q. J. Roy. Meteorol. Soc.*, 124, 1465–1484, 1998. 29699

Stohl, A., Wotawa, G., Seibert, P., and Kromp-Kolb, H.: Interpolation errors in wind fields as a function of spatial and temporal resolution and their impact on different types of kinematic trajectories, *J. Appl. Meteorol.*, 34, 2149–2165, 1995. 29699

Swietlicki, E., Hansson, H. C., Hameri, K., Svenningsson, B., Massling, A., McFiggans, G.,

Aerosol extinction coefficients at ambient conditions

P. Zieger et al.

[Title Page](#)[Abstract](#)[Introduction](#)[Conclusions](#)[References](#)[Tables](#)[Figures](#)[◀](#)[▶](#)[◀](#)[▶](#)[Back](#)[Close](#)[Full Screen / Esc](#)[Printer-friendly Version](#)[Interactive Discussion](#)

McMurry, P. H., Petaja, T., Tunved, P., Gysel, M., Topping, D., Weingartner, E., Baltensperger, U., Rissler, J., Wiedensohler, A., and Kulmala, M.: Hygroscopic properties of submicrometer atmospheric aerosol particles measured with H-TDMA instruments in various environments – a review, *Tellus*, 60B, 432–469, 2008. 29694

5 Van Roozendael, M., Fayt, C., Post, P., Hermans, C., and Lambert, J.-C.: Retrieval of BrO and NO₂ from UV-Visible Observations, in: *Sounding the troposphere from space: a new era for atmospheric chemistry*, Springer-Verlag, ISBN 3-540-40873-8, edited by: Borell, P., Borrell, P. M., Burrows, J. P., and Platt, U., 2003. 29694

10 Voss, K. J., Welton, J. E. J., Quinn, P. K., Frouin, R., Miller, M., and Reynolds, R. M.: Aerosol optical depth measurements during the Aerosols99 experiment, *J. Geophys. Res.*, 106(D18), 20811–20819, 2001. 29688

15 Wagner, T., Dix, B., Friedeburg, v.C., Frieß, U., Sanghavi, S., Sinreich, R., and Platt, U.: MAX-DOAS O₄ measurements: A new technique to derive information on atmospheric aerosols Principles and information content, *J. Geophys. Res.*, 109, D22205, doi:10.1029/2004JD004904, 2004. 29694

20 Wagner, T., Deutschmann, T., and Platt, U.: Determination of aerosol properties from MAX-DOAS observations of the Ring effect, *Atmos. Meas. Tech.*, 2, 495–512, doi:10.5194/amt-2-495-2009, 2009. 29695

25 Wagner, T., Beirle, S., Brauers, T., Deutschmann, T., Halla, J., Hak, C., Heue, K. P., Junckermann, W., Li, X., Pundt, I., Frieß, U., and Platt, U.: Inversion of tropospheric profiles of aerosol extinction and HCHO and NO₂ concentrations from MAX-DOAS observations in Milano in summer 2003 and comparison with independent data sets, in preparation, 2010. 29721

30 Wang, W., Rood, M. J., Carrico, C. M., Covert, D. S., Quinn, P. K., and Bates, T. S.: Aerosol optical properties along the northeast coast of North America during the New England Air Quality Study – Intercontinental Transport and Chemical Transformation 2004 campaign and the influence of aerosol composition, *J. Geophys. Res.*, 112, D10S23, doi:10.1029/2006JD007579, 2007. 29687

Weingartner, E., Burtscher, H., and Baltensperger, U.: Hygroscopic properties of carbon and diesel soot particles, *Atmos. Environ.*, 31(15), 2311–2327, 1997. 29701

Weingartner, E., Saathoff, H., Schnaiter, M., Streit, N., Bitnar, B., and Baltensperger, U.: Absorption of light by soot particles: Determination of the absorption coefficient by means of aethalometers, *J. Aerosol Sci.*, 34, 1445–1465, 2003. 29692

Winklmayr, W., Reischl, G., Lindner, A., and Berner, A.: A new electromobility spectrometer for the measurement of aerosol size distributions in the size range from 1 to 1000 nm, *J. Aerosol Sci.*, 22(3), 289–296, doi:10.1016/S0021-8502(05)80007-2, 1991. 29693

Wittrock, F., Oetjen, H., Richter, A., Fietkau, S., Medeke, T., Rozanov, A., and Burrows, J. P.: MAX-DOAS measurements of atmospheric trace gases in Ny-Ålesund – Radiative transfer studies and their application, *Atmos. Chem. Phys.*, 4, 955–966, doi:10.5194/acp-4-955-2004, 2004. 29694

WMO/GAW: Aerosol Measurement Procedures Guidelines and Recommendations, World Meteorological Organization Global Atmosphere Watch, Geneva, Switzerland, 2003. 29686

Yan, P., Pan, X. L., Tang, J., Zhou, X. J., Zhang, R. J., and Zeng, L. M.: Hygroscopic growth of aerosol scattering coefficient: a comparative analysis between urban and suburban sites at winter in Beijing, *Particuology*, 7, 52–60, 2009. 29687

York, D., Evensen, N. M., Lopez Martinez, M., and De Basabe Delgado, J.: Unified equations for the slope, intercept, and standard errors of the best straight line, *Am. J. Phys.*, 72(3), 367–375, 2004. 29703, 29707

Zieger, P., Fierz-Schmidhauser, R., Gysel, M., Ström, J., Henne, S., Yttri, K. E., Baltensperger, U., and Weingartner, E.: Effects of relative humidity on aerosol light scattering in the Arctic, *Atmos. Chem. Phys.*, 10, 3875–3890, doi:10.5194/acp-10-3875-2010, 2010. 29687, 29701, 29702, 29704

Aerosol extinction coefficients at ambient conditionsP. Zieger et al.

[Title Page](#)[Abstract](#)[Introduction](#)[Conclusions](#)[References](#)[Tables](#)[Figures](#)[◀](#)[▶](#)[◀](#)[▶](#)[Back](#)[Close](#)[Full Screen / Esc](#)[Printer-friendly Version](#)[Interactive Discussion](#)

Aerosol extinction coefficients at ambient conditions

P. Zieger et al.

Table 1. Overview of the main MAX-DOAS technical and inversion properties.

	BIRA ^a	IUPHD ^b	JAMSTEC ^c	MPI ^d
Wavelength	400–700 nm	290–790 nm	223–558 nm	310–461 nm
Spectral resolution (FWHM)	0.95 nm	0.5–0.6 nm	0.7 nm	0.5–0.9 nm
Field of view	0.8°	0.9°	<1°	1.2°
O ₄ bands used	477 nm	477 nm	477 nm	360 nm
Scaling factor	0.75	0.8	0.8	0.83
Elevation angles (°)	1, 2, 4, 5, 8, 10, 15, 30, 90	2, 4, 8, 15, 30, 90	2, 4, 8, 15, 30, 90 ^e	2, 4, 6, 8, 10, 15, 30, 90
Inversion scheme	Optimal estimation	Optimal estimation	Optimal estimation	Least squares
Time resolution	15 min	15 min	30 min	10 min
	1 elevation sequence	2–3 elevation sequences	1 elevation sequence	1 elevation sequence
Radiative transfer model	LIDORT v3.3 ^f	SCIATRAN ^g	MCARaTS ^h	McARTim ⁱ
Aerosol optical properties	AERONET ^j , in-situ	OPAC ^k	ω_0 : 0.95, AP: 0.65 ^l	ω_0 : 0.95, AP: 0.68
Time period used	19.6.–21.7.	23.6.–26.9.	19.6.–24.7.	22.6.–14.7.
Vertical discretization	200 m	200 m	1 km	20–5000 m

^a Clémer et al. (2010); ^b Frieß et al. (2006); ^c Irie et al. (2008, 2009); ^d Li et al. (2010); Wagner et al. (2010); ^e from 08.06.–21.06. 3° was used instead of 2°; ^f Spurr (2008); ^g Rozanov et al. (2001); ^h Iwabuchi (2006); ⁱ Deutschmann and Wagner (2008); ^j Holben et al. (1998); ^k Calculated for an assumed mixture of water soluble and soot particles (Hess et al., 1998); ^l ω_0 : single scattering albedo, AP: asymmetry parameter

Title Page

Abstract

Introduction

Conclusions

References

Tables

Figures

◀

▶

◀

▶

Back

Close

Full Screen / Esc

Printer-friendly Version

Interactive Discussion



Aerosol extinction coefficients at ambient conditions

P. Zieger et al.

Title Page

Abstract

Introduction

Conclusions

References

Tables

Figures

⏪

⏩

◀

▶

Back

Close

Full Screen / Esc

Printer-friendly Version

Interactive Discussion



Table 2. Results of an orthogonal linear regression (using weights) between ambient in-situ and MAX-DOAS extinction coefficients for the time periods given in Table 1. Values in parenthesis are for time periods when all four MAX-DOAS instruments were measuring in parallel.

	BIRA with Cimel	BIRA with in-situ	IUPHD	JAMSTEC	MPI
Slope	3.4 (2.9)	2.7 (2.4)	2.9 (2.2)	3.4 (2.6)	1.5 (1.2)
Error slope	0.06 (0.08)	0.04 (0.06)	0.05 (0.06)	0.06 (0.09)	0.08 (0.2)
Intercept	-1.6×10^{-5} (-2.4×10^{-5})	-8.2×10^{-6} (-1.3×10^{-5})	-1.2×10^{-5} (1.2×10^{-5})	-2.9×10^{-6} (1.4×10^{-5})	4.6×10^{-5} (4.3×10^{-5})
Error intercept	2×10^{-6} (3×10^{-6})	1×10^{-6} (2×10^{-6})	2×10^{-6} (4×10^{-6})	2×10^{-6} (3×10^{-6})	8×10^{-6} (2×10^{-5})
No. of points	404 (124)	362 (132)	830 (177)	629 (96)	642 (194)
R^2	0.78 (0.79)	0.81 (0.83)	0.66 (0.76)	0.74 (0.75)	0.62 (0.72)

Aerosol extinction coefficients at ambient conditions

P. Zieger et al.

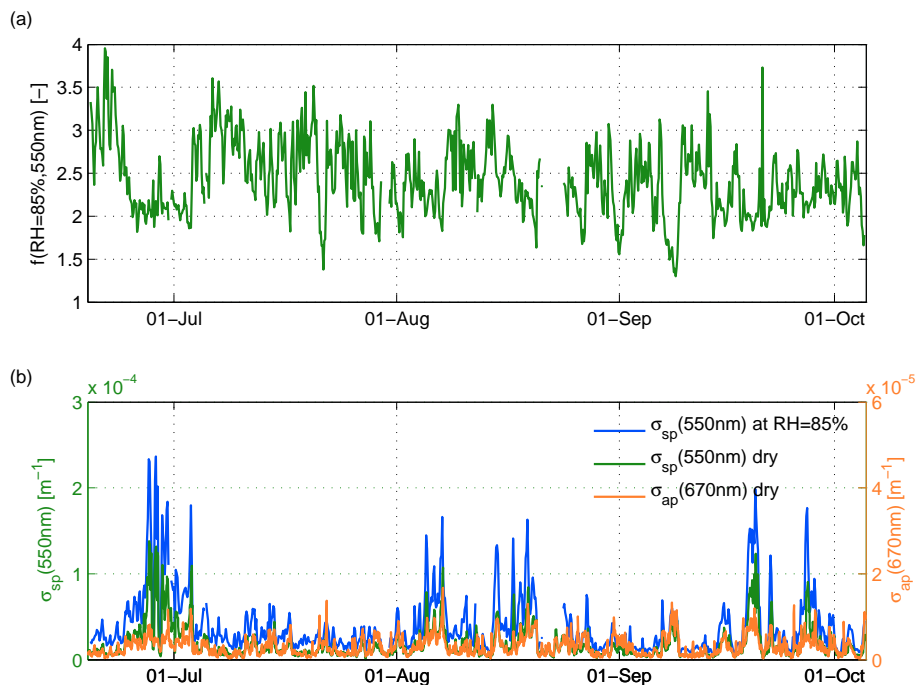


Fig. 1. Panel (a) Time series of the scattering enhancement factor $f(\text{RH} = 85\%, 550 \text{ nm})$ measured at Cabauw, The Netherlands, during summer and fall 2009. Panel (b) Scattering coefficient at $\lambda = 550 \text{ nm}$ at $\text{RH} = 85\%$ (blue line) and at dry conditions (green line) measured by the humidified nephelometer (WetNeph) and reference nephelometer (DryNeph). The absorption coefficient at $\lambda = 670 \text{ nm}$ (orange line) was measured by the multi-angle absorption photometer (MAAP) at dry conditions.

Title Page

Abstract

Introduction

Conclusions

References

Tables

Figures

◀

▶

◀

▶

Back

Close

Full Screen / Esc

Printer-friendly Version

Interactive Discussion



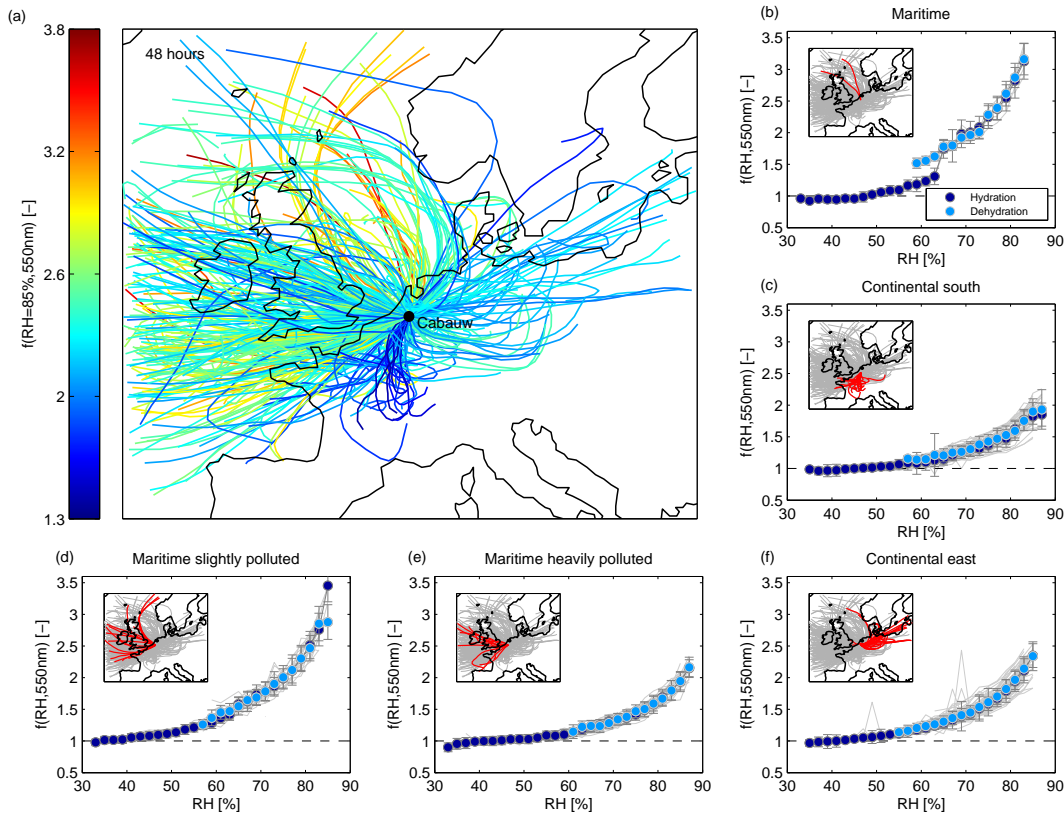


Fig. 2. Panel **(a)** FLEXTRA trajectories (48 h backward calculation) of air parcels arriving at Cabauw. The trajectories are color coded with the mean scattering enhancement $f(\text{RH} = 85\%, 550 \text{ nm})$ measured at the site. Panels **(b)–(f)** Example humidograms classified by the origin of the air masses. Dark blue circles denote averages of $f(\text{RH})$ for the hydration branch of the humidogram, while light blue circles are averages of the dehydration branch (2% RH bins). Underlined in grey are the individual humidograms of each trajectory. Error bars denote the standard deviation.

Aerosol extinction coefficients at ambient conditions

P. Zieger et al.

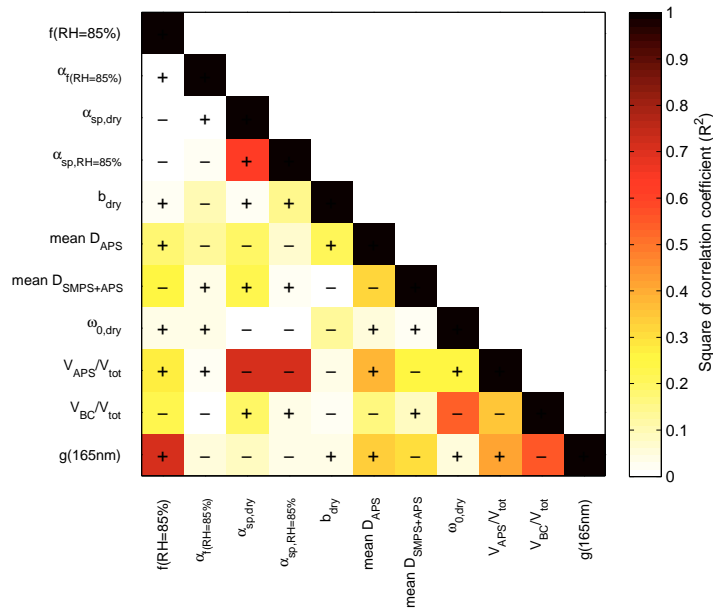


Fig. 3. Correlation plot of all intensive aerosol parameters measured in-situ at the Cabauw tower. $f(\text{RH} = 85\%, 550 \text{ nm})$: scattering enhancement factor; $\alpha_{f(\text{RH})}$: Ångström exponent of $f(\text{RH} = 85\%, 550 \text{ nm})$; $\alpha_{\text{sp,dry}}$: Ångström exponent of scattering coefficient at low RH; $\alpha_{\text{sp,RH}=85\%}$: Ångström exponent of scattering coefficient at RH = 85%; b_{dry} : backscatter fraction (at $\lambda = 550 \text{ nm}$) at low RH; D_{APS} : mean (dry) diameter of APS size distribution measurement; D_{SMPS} : mean (dry) diameter of SMPS size distribution measurement; $\omega_{0,\text{dry}}$: single scattering albedo at low RH (at $\lambda = 550 \text{ nm}$); $V_{\text{APS}}/V_{\text{tot}}$: coarse mode fraction measured by APS and SMPS; $V_{\text{BC}}/V_{\text{tot}}$: black carbon volume fraction measured by MAAP, SMPS, and APS; $g(165 \text{ nm})$: hygroscopic growth factor measured at the dry diameter $d_0 = 165 \text{ nm}$ and at RH = 90% by the H-TDMA. Plus and minus signs indicate the slope of the regression line.

Title Page

Abstract

Introduction

Conclusions

References

Tables

Figures

◀

▶

◀

▶

Back

Close

Full Screen / Esc

Printer-friendly Version

Interactive Discussion



Aerosol extinction coefficients at ambient conditions

P. Zieger et al.

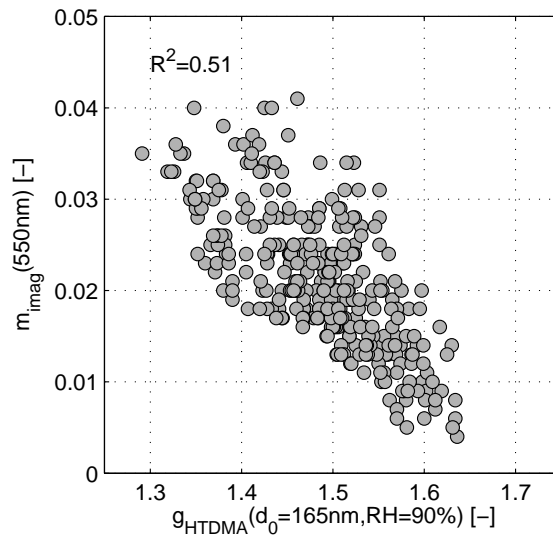


Fig. 4. Retrieved imaginary part of the complex refractive index versus the hygroscopic growth factor measured by the H-TDMA (at $d_0 = 165$ nm and RH = 90%).

Title Page

Abstract

Introduction

Conclusions

References

Tables

Figures

◀

▶

◀

▶

Back

Close

Full Screen / Esc

Printer-friendly Version

Interactive Discussion



Aerosol extinction coefficients at ambient conditions

P. Zieger et al.

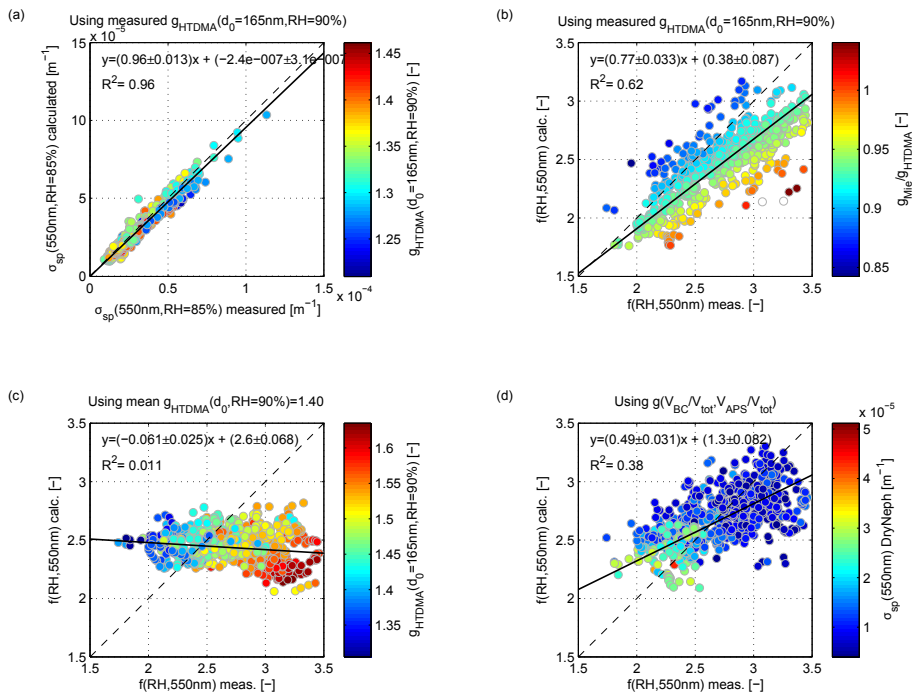


Fig. 5. Panel (a) Scattering coefficient σ_{sp} calculated vs. measured using the hygroscopic growth factor measured by the H-TDMA. Panel (b)–(d) Scattering enhancement factor $f(\text{RH} = 85\%, 550 \text{ nm})$ calculated vs. measured values. Panel (b) The measured hygroscopic growth factor of the H-TDMA (dry diameter $d_0 = 165 \text{ nm}$) has been used for the calculation, the colorcode denotes the ratio of g_{Mie}/g_{HTDMA} . Panel (c) A fixed value of $g(\text{RH} = 85\%) = 1.4$ (mean for that period) has been used for the calculation. Panel (d) An empirical relation of $g(V_{BC}/V_{tot}, V_{APS}/V_{tot})$ has been used for the calculation of $f(\text{RH})$. All values are shown at $\text{RH} = 85\%$. The solid black line represents a bivariate linear regression including weights (with calculated uncertainty of slope and intercept). The 1:1-line is shown as a dashed line.

Title Page

Abstract

Introduction

Conclusions

References

Tables

Figures



Back

Close

Full Screen / Esc

Printer-friendly Version

Interactive Discussion



Aerosol extinction coefficients at ambient conditions

P. Zieger et al.

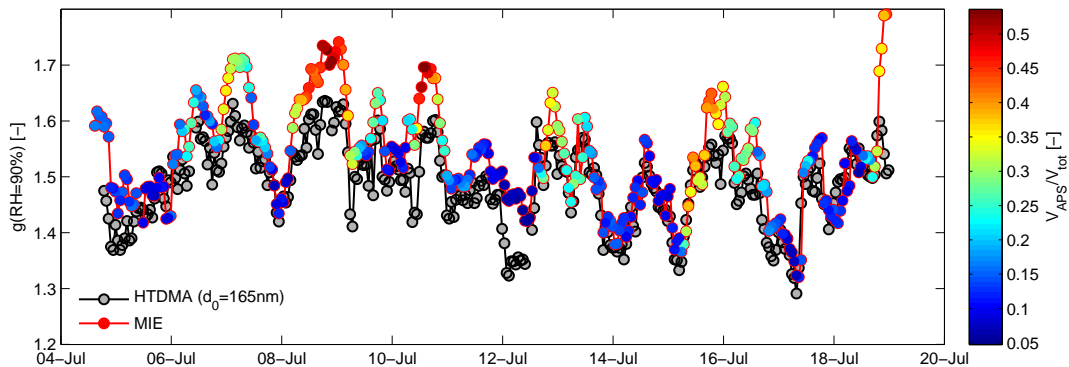


Fig. 6. Time series of the hygroscopic growth factor measured by the H-TDMA (black line) and retrieved from WetNeph, DryNeph, SMPS, APS measurements and Mie theory (red line). The color code denotes the volume coarse mode fraction measured by the APS and SMPS.

[Title Page](#)[Abstract](#)[Introduction](#)[Conclusions](#)[References](#)[Tables](#)[Figures](#)[⏪](#)[⏩](#)[◀](#)[▶](#)[Back](#)[Close](#)[Full Screen / Esc](#)[Printer-friendly Version](#)[Interactive Discussion](#)

Aerosol extinction coefficients at ambient conditions

P. Zieger et al.

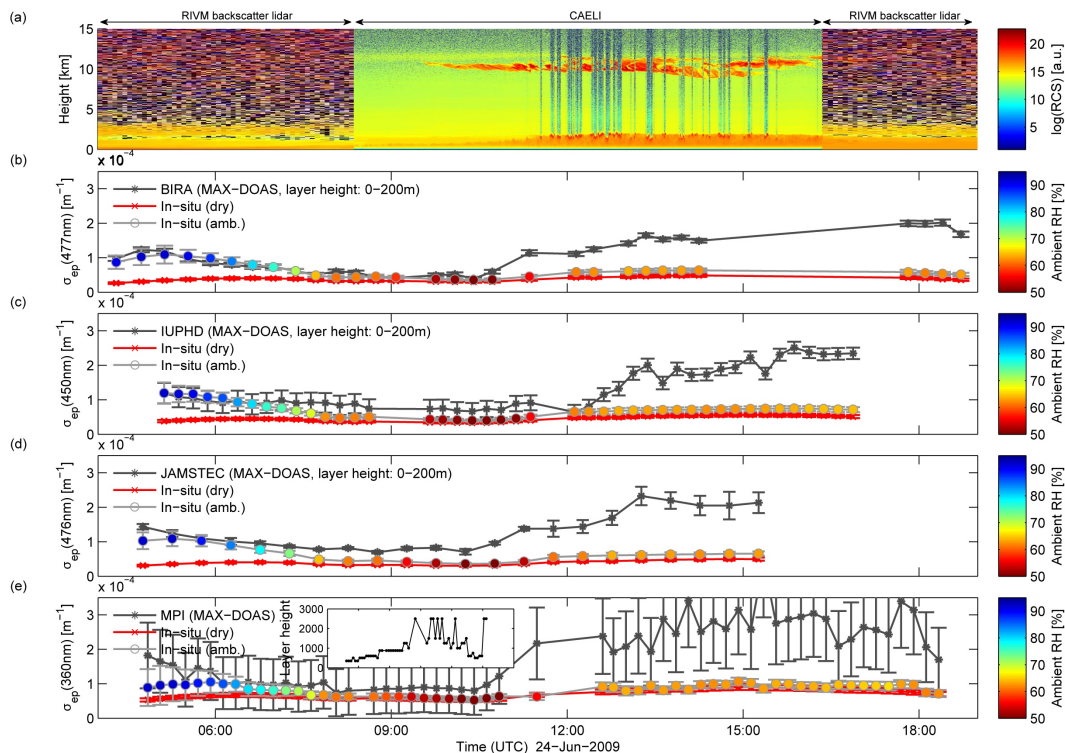


Fig. 7. Example day 24 June 2009 (golden day). Panel (a) Range corrected signal (RCS) at 1064 nm measured by the RIVM backscatter and the CAELI lidar. Panels (b)–(e) Time series of the aerosol extinction coefficient retrieved by MAX-DOAS instruments (black line) compared to in-situ measurements (red line: dry in-situ extinction coefficient, grey line: ambient value at the RH denoted in the color coded dots).

Title Page

Abstract

Introduction

Conclusions

References

Tables

Figures

◀

▶

◀

▶

Back

Close

Full Screen / Esc

Printer-friendly Version

Interactive Discussion

Aerosol extinction coefficients at ambient conditions

P. Zieger et al.

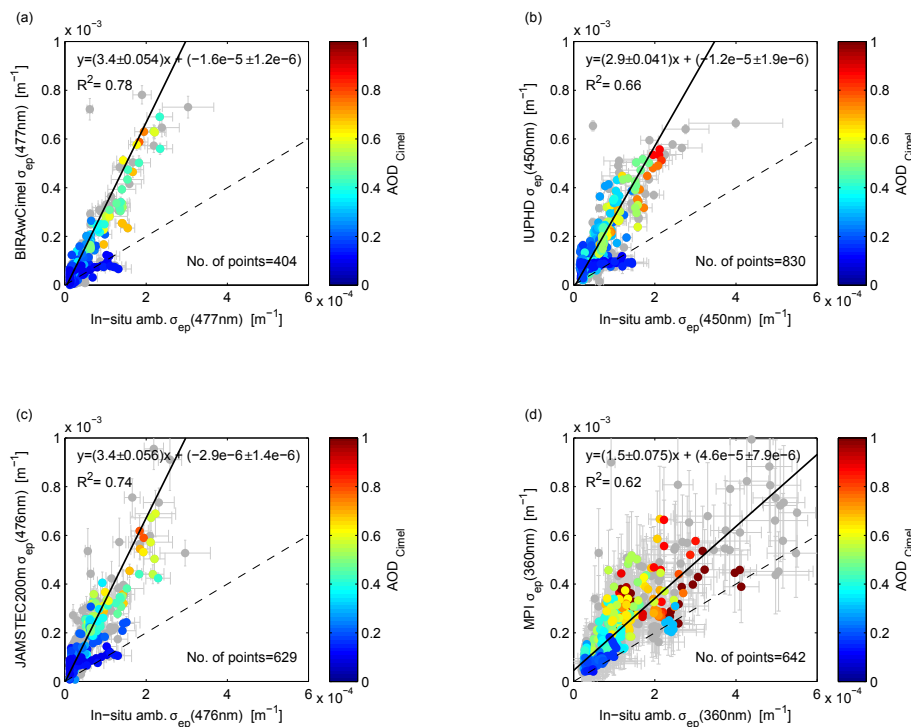


Fig. 8. Ambient extinction coefficient retrieved by MAX-DOAS vs. in-situ measurements brought to ambient conditions. The color code denotes the AOD measured by the Cimel sun photometer (AOD interpolated to the according wavelength; grey points are times with no sun photometer measurements). The solid black line represents a bivariate linear regression including weights (with calculated uncertainty of slope and intercept). The dashed line is the 1:1-line.

Title Page

Abstract

Introduction

Conclusions

References

Tables

Figures

◀

▶

◀

▶

Back

Close

Full Screen / Esc

Printer-friendly Version

Interactive Discussion



Aerosol extinction coefficients at ambient conditions

P. Zieger et al.

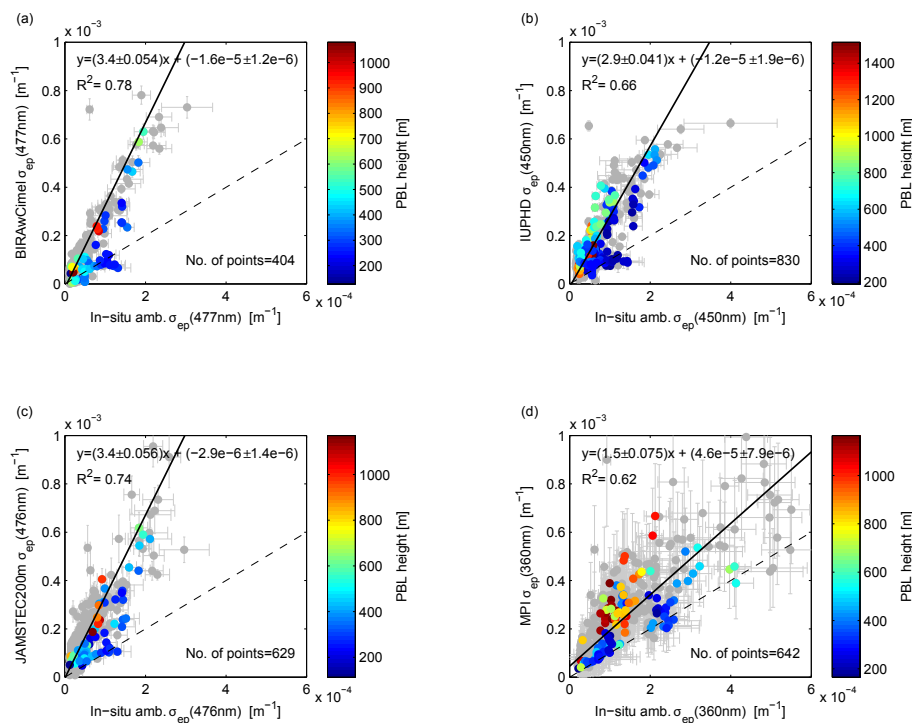


Fig. 9. Same as Fig. 8, but here the color code denotes the planetary boundary layer height measured by the ceilometer (grey points: no quality assured PBL data available).

Title Page

Abstract

Introduction

Conclusions

References

Tables

Figures

◀

▶

◀

▶

Back

Close

Full Screen / Esc

Printer-friendly Version

Interactive Discussion



Aerosol extinction coefficients at ambient conditions

P. Zieger et al.

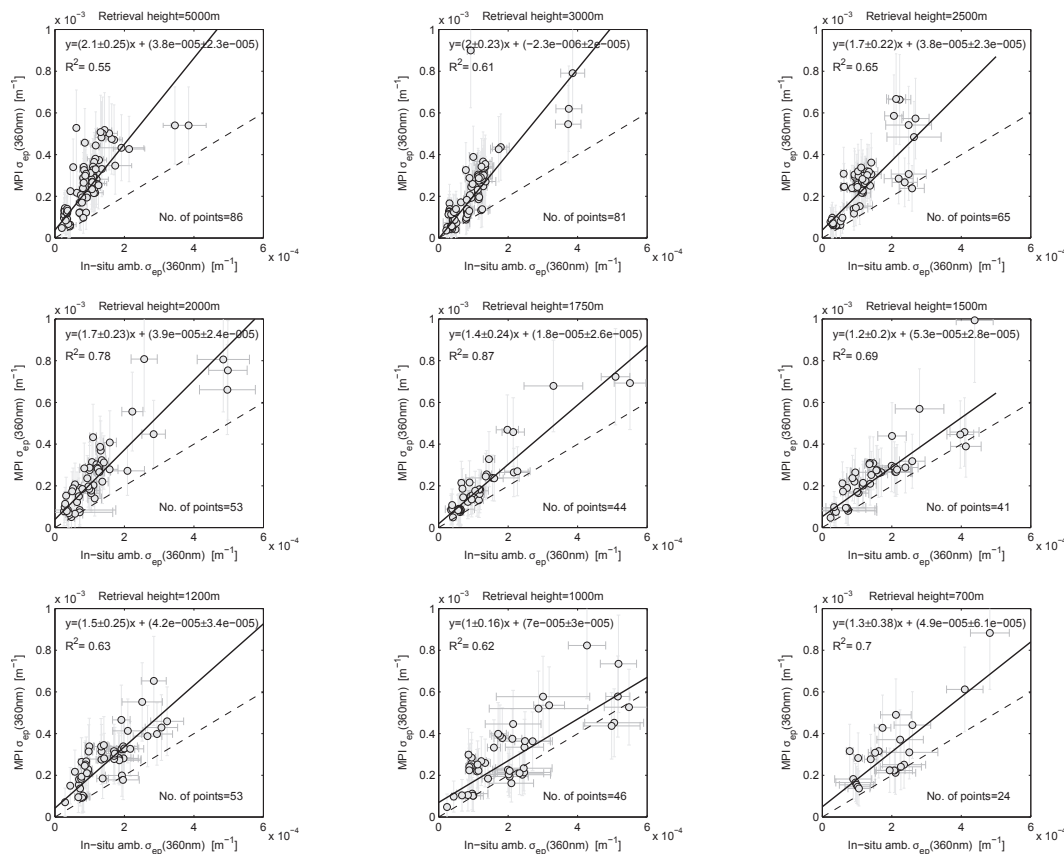


Fig. 10. Ambient extinction coefficient measured by the MPI MAX-DOAS instrument, where the layer height is kept variable during the MAX-DOAS retrieval vs. in-situ. The aerosol type is assumed to be constant within the layer (for the calculation of the in-situ σ_{ep} , only the RH changes with height). The RH profiles are taken from assimilated COSMO data. Solid line represents a bivariate linear regression including weights (with calculated uncertainty of slope and intercept), dashed line is the 1:1-line. 29732

Title Page

Abstract

Introduction

Conclusions

References

Tables

Figures

◀

▶

◀

▶

Back

Close

Full Screen / Esc

Printer-friendly Version

Interactive Discussion



Aerosol extinction coefficients at ambient conditions

P. Zieger et al.

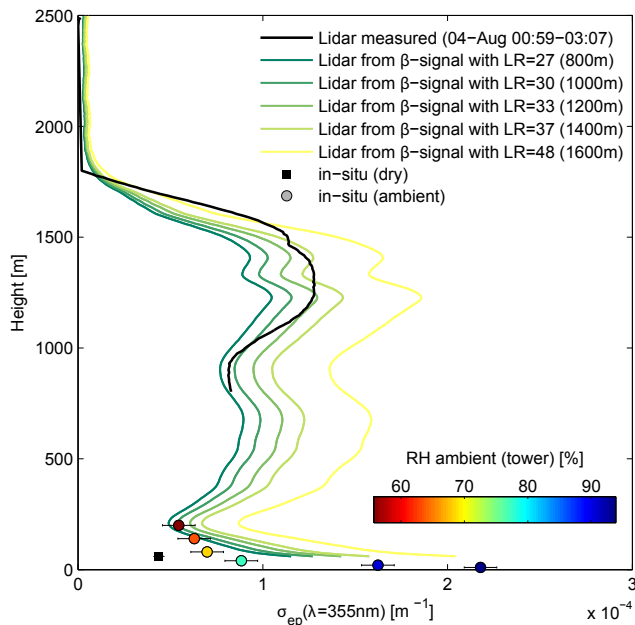


Fig. 11. Lidar and in-situ measurements of the aerosol extinction coefficient σ_{ep} at $\lambda = 355 \text{ nm}$ (4 August 2009, 00:59–03:07). Black line: Direct lidar measurement of σ_{ep} ; Colored lines: σ_{ep} calculated from the backscatter signal using measured lidar ratios (LR) obtained from mean values of different height levels ($\pm 100 \text{ m}$); black square: σ_{ep} measured in-situ at dry conditions; colored circles: σ_{ep} brought to ambient conditions (color code denotes the ambient RH measured at the tower, error bars are retrieved via Gaussian error propagation).

Title Page

Abstract

Introduction

Conclusions

References

Tables

Figures

◀

▶

◀

▶

Back

Close

Full Screen / Esc

Printer-friendly Version

Interactive Discussion



Aerosol extinction coefficients at ambient conditions

P. Zieger et al.

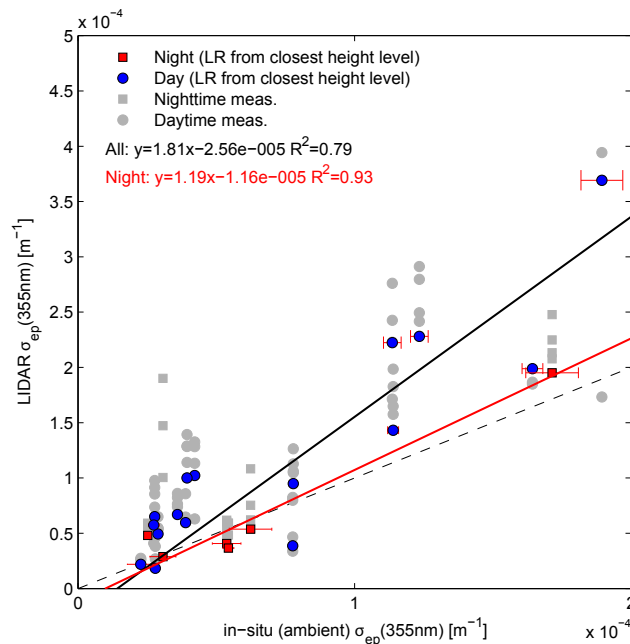


Fig. 12. Comparison of the ambient extinction coefficient measured by lidar vs. the in-situ measurement (mean values for ~60–200 m). The colored points denote the mean value, if the lidar ratio (LR) of the lowest possible height level is taken for extrapolation (error bars denote the standard deviation). Circles: daytime measurements; Squares: nighttime measurements. The solid black line represents an orthogonal least-square fit for all profiles (lowest possible LR taken for extrapolation). The red solid line represents the same regression for nighttime measurements only.

Title Page

Abstract

Introduction

Conclusions

References

Tables

Figures

◀

▶

◀

▶

Back

Close

Full Screen / Esc

Printer-friendly Version

Interactive Discussion

